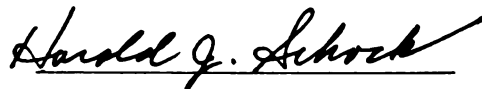




This is to certify that the
thesis entitled
**EXPERIMENTAL MEASUREMENTS OF
THE FLOW FIELD INSIDE OF AN
AUTOMOTIVE TORQUE CONVERTER**
presented by
Lawrence Joseph Dalimonte
has been accepted towards fulfillment
of the requirements for
M.S. degree in Mechanical Engineering



Major professor

Date 5/11/98

LIBRARY
Michigan State
University

PLACE IN RETURN BOX
to remove this checkout from your record.
TO AVOID FINES return on or before date due.

DATE DUE	DATE DUE	DATE DUE

**EXPERIMENTAL MEASUREMENTS OF
THE FLOW FIELD INSIDE OF AN
AUTOMOTIVE TORQUE CONVERTER**

By

Lawrence Joseph Dalimonte

A THESIS

**Submitted to
Michigan State University
in partial fulfillment of the requirements
for the degree of**

MASTER OF SCIENCE

Department of Mechanical Engineering

1998

ABSTRACT

EXPERIMENTAL MEASUREMENTS OF THE FLOW FIELD INSIDE OF AN AUTOMOTIVE TORQUE CONVERTER USING LASER DOPPLER VELOCIMETRY

By

Lawrence Joseph Dalimonte

The automotive torque converter flow fields are complex, in that they contain three-dimensional flows, which are viscous and unsteady. To add to the complexity, the difference in rotor speeds between the impeller and turbine compound the flow effects. The purpose of this study was to characterize the internal flow experimentally in a production torque converter from Ford Motor Company.

The flow characteristics were quantified by Laser Doppler Velocimetry (LDV) measurements. The LDV system was employed for this study because understanding the fluid flow is crucial for characterizing the flows at the measured points within the torque converter. LDV measurements were conducted at a total of 9 planes at two different speed ratios. Flows at the impeller exit and gap region were affected by the turbine blade as it passed. Fluid flow was also found to be leaving the impeller and flowing up behind the turbine, negatively effecting converter efficiency. Velocity profile animations were created using the measured velocity data and custom software to allow viewing on a unix workstation.

ACKNOWLEDGEMENTS

I would like to take this opportunity to express my sincere appreciation to those of whom made this study possible. First and foremost, to my wife Kim, and my children Lawrence II and Leann, for their patience and understanding during my academic career. Also to my parents Al and Fran Dalimonte, for their support and encouragement that continues to this day. To Tom Stuecken on his expertise in designing and building of experimental equipment; Dr. Keunchul Lee for his guidance with the LDV system and his knowledge of research in general; to Matt Foster for his help with the data management and processing, among other things; to Mark Novak for his work with Explorer making the animation of the velocity profiles possible; to Dr. Giles Brereton, Jon Darrow, Mahmood Rahi, Mikhail Ejakov, and Hans Hascher for their knowledge and advice on numerous other matters; and finally, to Dr. Harold Schock for making this opportunity not only possible, but a reality.

TABLE OF CONTENTS

LIST OF TABLES	vii
LIST OF FIGURES	viii
LIST OF SYMBOLS	xii
CHAPTER 1	
INTRODUCTION	1
1.1 Motivation	1
1.2 Torque Converter Fundamentals	2
1.3 Problem Statement	4
1.4 Literature Review	4
CHAPTER 2	
EXPERIMENTAL EQUIPMENT	9
2.1 Test Facility: Test Rig	9
2.2 Transmission Oil Supply System	10
2.3 Test Rig Controller	12
2.4 LDV System	12
CHAPTER 3	
TORQUE CONVERTER	18
3.1 Modification	18
3.2 Front Window	20
3.3 Side Window	21
CHAPTER 4	
EXPERIMENTAL PROCEDURE	23
4.1 Preliminary Testing	23
4.2 Setup	23
4.3 Data Acquisition	26
4.4 Measurements with Front Window: First Series	32
4.5 Measurements with Front Window: Second Series	33
4.6 Measurements with Side Window: Third Series	34
4.7 Side Window Geometry	36
4.8 Data Post Processing	39
4.9 Animation	45
CHAPTER 5	
RESULTS AND DISCUSSION	47
5.1 Measurements with Front Window: First Series (Planes 1-9) ..	47
5.1.1 Plane 1: 0.8 Speed Ratio	48

TABLE OF CONTENTS (CONT.)

5.1.2 Plane 1: 0.4 Speed Ratio	48
5.1.3 Plane 1: Comparison of Both Speed Ratios.....	49
5.1.4 Plane 2: 0.8 Speed Ratio	50
5.1.5 Plane 2: 0.4 Speed Ratio	50
5.1.6 Plane 2: Comparison of Both Speed Ratios.....	51
5.1.7 Plane 3: 0.8 Speed Ratio	52
5.1.8 Plane 3: 0.4 Speed Ratio	52
5.1.9 Plane 3: Comparison of Both Speed Ratios.....	53
5.2 Measured with Front Window: Second Series.....	53
5.2.1 Plane 4: 0.8 Speed Ratio	53
5.2.2 Plane 4: 0.4 Speed Ratio	54
5.2.3 Plane 4: Comparison of Both Speed Ratios.....	54
5.2.4 Plane 5: 0.8 Speed Ratio	55
5.2.5 Plane 5: 0.4 Speed Ratio	56
5.2.6 Plane 5: Comparison of Both Speed Ratios.....	57
5.3 Measurements with Side Window: Third Series (Planes 6-9)...	68
5.3.1 Plane 6: 0.8 Speed Ratio	68
5.3.2 Plane 6: 0.4 Speed Ratio	68
5.3.3 Plane 6: Comparison of Both Speed Ratios.....	68
5.3.4 Plane 7: 0.8 Speed Ratio	69
5.3.5 Plane 7: 0.4 Speed Ratio	69
5.3.6 Plane 7: Comparison of Both Speed Ratios.....	70
5.3.7 Plane 8: 0.8 Speed Ratio	70
5.3.8 Plane 8: 0.4 Speed Ratio	71
5.3.9 Plane 8: Comparison of Both Speed Ratios.....	71
5.3.10 Plane 9: 0.8 Speed Ratio	72
5.3.11 Plane 9: 0.4 Speed Ratio	73
5.3.12 Plane 9: Comparison of Both Speed Ratios.....	73
5.4 Data Comparison	83
5.4.1 Front Window: Planes 2 and 4 at Both Speed Ratios ..	83
5.5 Steady State Condition Velocity Analysis.....	88
5.5.1 Plane 1: Comparison of Both Speed Ratios.....	89
5.5.2 Plane 2: Comparison of Both Speed Ratios.....	90
5.5.3 Plane 3: Comparison of Both Speed Ratios.....	91
5.5.4 Plane 4: Comparison of Both Speed Ratios.....	91
5.5.5 Plane 5: Comparison of Both Speed Ratios.....	92
5.5.6 Plane 6: Comparison of Both Speed Ratios.....	93
5.5.7 Plane 7: Comparison of Both Speed Ratios.....	93
5.5.8 Plane 8: Comparison of Both Speed Ratios.....	94
5.5.9 Plane 9: Comparison of Both Speed Ratios.....	95
5.6 Mass Flow Rates	114

TABLE OF CONTENTS (CONT.)

5.6.1 Mass Flow Rates: Plane 1	115
5.6.2 Mass Flow Rates: Plane 6	115
5.6.3 Mass Flow Rates: Plane 7	116
5.6.4 Mass Flow Rates: Plane 8	116
5.6.5 Mass Flow Rates: Plane 9	117
CHAPTER 6	
SUMMARY AND CONCLUSIONS	125
CHAPTER 7	
RECOMMENDATIONS	128
LIST OF REFERENCES	130

LIST OF TABLES

Table 1. Ford production torque converter specifications	19
Table 2. Measured plane locations in Ford coordinate system	29
Table 3. Test conditions for data measured	31

LIST OF FIGURES

Figure 1. Torque converter assembly.....	3
Figure 2. View of Test Rig	10
Figure 3. Transmission Oil Supply System.....	11
Figure 4. VI screen display	13
Figure 5. Test Rig and Test Rig Controller	14
Figure 6. View of 4-beam probe of LDV system and test rig with front window converter.....	14
Figure 7. 4-beam probe with fringe pattern	15
Figure 8. View of impeller half of converter with front window installed.....	19
Figure 9. View of front window.....	20
Figure 10. View of impeller half of converter with side window installed.....	22
Figure 11. View of test rig apparatus for traverse table reference point	25
Figure 12. View of Impeller and turbine positions for encoder references	26
Figure 13. Impeller and turbine blades inside the torque converter with measured planes (Ford coordinate system).....	28
Figure 14. View of measured vector components in both front and side window series	30

LIST OF FIGURES (CONT.)

Figure 15. First Series with 3 planes	33
Figure 16. Second Series with 2 planes	34
Figure 17. Third Series with 4 planes.....	35
Figure 18. View of side window	36
Figure 19. View of beam focal point through the side window	38
Figure 20. 3-D display of side window (Demmer).....	38
Figure 21. Data acquisition flow chart	40
Figure 22. Data processing flow chart.....	41
Figure 23. Plane 1 (mid-chord of impeller) at 0.8 speed ratio.....	58
Figure 24. Plane 1 (mid-chord of impeller) at 0.4 speed ratio.....	59
Figure 25. Plane 2 (impeller exit) at 0.8 speed ratio.....	60
Figure 26. Plane 2 (impeller exit) at 0.4 speed ratio.....	61
Figure 27. Plane 3 (1mm inside turbine) at 0.8 speed ratio	62
Figure 28. Plane 3 (1mm inside turbine) at 0.4 speed ratio	63
Figure 29. Plane 4 (impeller exit) at 0.8 speed ratio.....	64
Figure 30. Plane 4 (impeller exit) at 0.4 speed ratio.....	65
Figure 31. Plane 5 (1mm from impeller exit in gap region) at 0.8 speed ratio	66
Figure 32. Plane 5 (1mm from impeller exit in gap region) at 0.4 speed ratio	67
Figure 33. Plane 6 (2mm inside impeller) at 0.8 speed ratio.....	75

LIST OF FIGURES (CONT.)

Figure 34. Plane 6 (2mm inside impeller) at 0.4 speed ratio.....	76
Figure 35. Plane 7 (2mm inside impeller) at 0.8 speed ratio.....	77
Figure 36. Plane 7 (2mm inside impeller) at 0.4 speed ratio.....	78
Figure 37. Plane 8 (impeller exit) at 0.8 speed ratio.....	79
Figure 38. Plane 8 (impeller exit) at 0.4 speed ratio.....	80
Figure 39. Plane 9 (1mm from impeller exit in gap region) at 0.8 speed ratio	81
Figure 40. Plane 9 (1mm from impeller exit in gap region) at 0.4 speed ratio.....	82
Figure 41. Comparison of planes 2 and 4 (both located at impeller exit) at 0.8 speed ratio	85
Figure 42. Comparison of planes 2 and 4 (both located at impeller exit) at 0.4 speed ratio	86
Figure 43. Comparison of planes 1 and 4 at 0.4 speed ratio	87
Figure 44. Steady state condition velocities plane 1 at 0.8 speed ratio ...	96
Figure 45. Steady state condition velocities plane 1 at 0.4 speed ratio ...	97
Figure 46. Steady state condition velocities plane 2 at 0.8 speed ratio ...	98
Figure 47. Steady state condition velocities plane 2 at 0.4 speed ratio ...	99
Figure 48. Steady state condition velocities plane 3 at 0.8 speed ratio .	100
Figure 49. Steady state condition velocities plane 3 at 0.4 speed ratio .	101
Figure 50. Steady state condition velocities plane 4 at 0.8 speed ratio .	102

LIST OF FIGURES (CONT.)

Figure 51. Steady state condition velocities plane 4 at 0.4 speed ratio .	103
Figure 52. Steady state condition velocities plane 5 at 0.8 speed ratio .	104
Figure 53. Steady state condition velocities plane 5 at 0.4 speed ratio .	105
Figure 54. Steady state condition velocities plane 6 at 0.8 speed ratio .	106
Figure 55. Steady state condition velocities plane 6 at 0.4 speed ratio .	107
Figure 56. Steady state condition velocities plane 7 at 0.8 speed ratio .	108
Figure 57. Steady state condition velocities plane 7 at 0.4 speed ratio .	109
Figure 58. Steady state condition velocities plane 8 at 0.8 speed ratio .	110
Figure 59. Steady state condition velocities plane 8 at 0.4 speed ratio .	111
Figure 60. Steady state condition velocities plane 9 at 0.8 speed ratio .	112
Figure 61. Steady state condition velocities plane 9 at 0.4 speed ratio .	113
Figure 62. Mass flow rate plane 1 at both speed ratios	119
Figure 63. Mass flow rate plane 6 at both speed ratios	120
Figure 64. Mass flow rate plane 7 at both speed ratios	121
Figure 65. Mass flow rate plane 8 at both speed ratios	122
Figure 66. Mass flow rate plane 9 at both speed ratios	123
Figure 67. Mass flow rate comparison planes 1, 6-9 both speed ratios..	124

LIST OF SYMBOLS

d_f	Fringe spacing
f	Focal length of transmitting lens
F	Doppler shift frequency of the scattered light
t_1	Time taken for the particle to cross a pair of fringes
κ	Beam half angle
λ	Wavelength of the laser beam

CHAPTER 1

INTRODUCTION

1.1 Motivation

The purpose of this study was to characterize the internal flow experimentally in a production torque converter from Ford Motor Company under known macroscopic operating conditions. Torque converter flow fields are complex, in that they contain three-dimensional flows, are viscous, and unsteady. To add to the complexity, the difference in rotor speeds between the impeller and turbine compound the flow effects. Few turbomachines, other than the hydraulic torque converter, operate with such a complex interface.

Two production torque converters of the same type were modified for this study. One converter was modified with a front window, and the other a side window. Both windows were installed in a housing mounted on the converter shell, which allowed optical access into the converter passages. The front window allows optical access into the impeller passage, between the impeller and turbine (gap region) and turbine. The side window allows optical access into the exit region of the impeller passage, gap region, and turbine from a different perspective.

The flow characteristics were quantified by Laser Doppler Velocimetry (LDV) measurements. The LDV system was employed for this study because a detailed understanding of the fluid flow is necessary for improved design of the torque converter. Also, the LDV system is a non-intrusive form of measuring with no calibration for temperature, density, etc., necessary. LDV measurements were conducted at a total of 9 planes. The measurements were conducted under two operating conditions, which were speed ratios of 0.4 and 0.8. The 0.4 speed ratio has an impeller speed of 1600 rpm and a turbine speed of 633 rpm, while the impeller speed is 2000 rpm and the turbine speed is 1600 rpm for the 0.8 speed ratio.

Velocity profile animations were created using the measured velocity data on a Silicon Graphics (SGI) computer. These animations, which show the ensemble averaged velocity profiles, compare data in plane to plane format. The overall efficiency of the torque converter may be improved by optimizing flow fields measured using internal flow diagnostics.

1.2 Torque Converter Fundamentals

The torque converter has three important functions. The first is that it must transfer power smoothly and efficiently from the engine to the transmission. Second, the torque converter must have the ability to

multiply engine torque for improved vehicle launching at low speeds. Third, it must be able to effectively dampen engine torsional vibrations and shock loads. The automotive torque converter is made up of several components (Figure 1). The impeller, also known as a pump, is attached directly to the cover. The cover, in turn, is connected to a flexplate, which is attached to the engine, and rotates at engine speed. When the converter is rotating fluid exits the impeller and impacts the turbine causing it to rotate. The turbine is driven by the impeller and rotates on its own axis driving the transmission input shaft. The stator is positioned between the impeller and turbine and redirects the fluid flow from the turbine to the impeller.

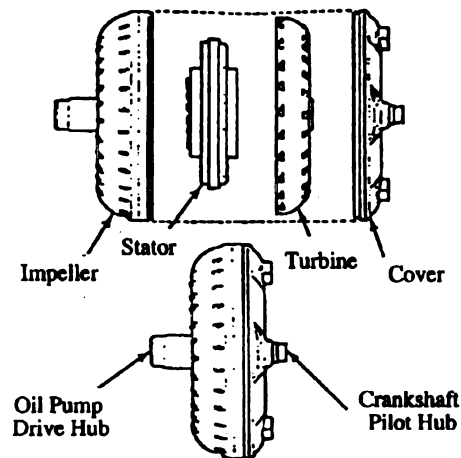


Figure 1. Torque converter assembly

1.3 Problem Statement

The objectives of this study centers on design technology improvements. Specific objectives include improving performance of the torque converter, reducing the length of the torque converter for automobile use with transverse engines, and reducing fuel consumption in urban use. To be able to achieve these objectives a thorough understanding of the fluid flows dynamic phenomena is essential. The use of LDV measurements make it possible to examine the internal flow characteristics of the torque converter.

1.4 Literature Review

The LDV system offers a non-intrusive form of measurement for flow characterization, thereby having provided data in numerous studies [1-4]. By and Mahoney (1988) summarized the technology needs for the automotive torque converter [5]. They suggested that the flow is highly three-dimensional due, in part, to complex geometries with three components rotating at different speeds. This makes the understanding of general fluid flow characteristics difficult. They conclude that internal flow analysis can be used to determine the physical flow phenomena associated with flow losses inside the converter.

Fister and Adrian (1983) were the first to measure the flow field in a torque converter, even though the converters were larger industrial units [6]. They used Laser-Two-Focus (L2F) and Spark Tracer methods in two geometrically identical and hydrodynamically similar torque converters. The L2F method used sight-holes and can only be applied to transparent fluids. The Spark Tracer method can only be applied in gases, requiring transparent and non-conductive walls. Therefore one converter was used with water as the operating fluid and second converter used air. The results are somewhat limited in comparison since not only are they not true automotive torque converters, the operating fluids used were not transmission oil.

By and Lakshminarayana (1995) measured the parameters of a torque converter pump and the static pressure field using eight static pressure probes [7]. The importance was stressed to measure static pressures under constant turbine/impeller speed ratio conditions, avoiding transient conditions. They found that the static pressure distribution generally poor and fluid separation at the core section under all speed ratio conditions.

Lakshminarayana and von Backstrom (1996) discuss different techniques in investigating the fluid flows inside of a torque converter [8]. These include laser velocimetry, hot wire velocimetry, fast response probes, conventional five-hole probes, as well as blade and wall static pressure measurements. They conclude that torque converter flows are

extremely complex and that methods developed need to be able to measure regions of flow separation and secondary flow circulation.

Watanabe et al. (1997) used a flow visualization and measurement of torque converter stator blades with laser sheet lighting methods and LDV [9]. The apparatus included a shaft with an open space housing a window and mirror so fluid flow in the stator could be directly observed. This study also involved varying the thickness of the stator blades. This was a proposed new experimental apparatus to visualize and measure the flow inside of the torque converter; since no known published case of applying a flow visualization or measurement technique with an actual torque converter was available. They concluded that the thickness of the stator blade does affect the torque capacity coefficient characteristics more than the efficiency and torque ratio characteristics.

Bahr et al. (1990) used a torque converter constructed entirely from Plexiglas and measured flow with an LDV system [10]. The data measured included the effect of instantaneous turbine and blade positions on the average velocity fields through the use of shaft encoders. This was an attempt to map flow characteristics in torque converter operating conditions. The constraint was that the rotor speeds were reduced due to the nature of the material used. They measured at two different speed ratios and found that the instantaneous turbine and impeller blades had a strong effect on the average velocity field in the stator. They also concluded that the torque is very poorly distributed at the upper half of

the blade. Therefore the blade should be redesigned for a more uniform flow and less flow separation.

There have been numerous studies on the operation of torque converters from CFD, pitot tube analysis to LDV measurements [11-20]. These were designed to understand fluid flow characteristics and improve torque converter performance. The shortcoming was none of the studies were performed in an actual automotive torque converter in realistic operating conditions.

McCarrick (1993) measured fluid flow fields in an actual automotive torque converter provided by Ford Motor Company [21]. The main emphasis of this study was to determine the feasibility and limitations of this method in mapping flow characteristics. Concentration began on the apparatus, which would both support and operate the converter during testing. It was necessary to make comparisons with numerical simulation and conduct testing under certain operating conditions that included the correct turbine/impeller ratios, as well as, proper flow rates and fluid temperatures. For maximum optical access within the converter the choice of material for the window was important. The refractive index of both the window material and oil used needed to be as close as possible. Development of an appropriate seeding method was also addressed in McCarrick's work. Reflectivity was as major an issue as were size and weight. Tests were conducted at 1000 and 1500 rpm at four different speed ratios. Data was recorded and processed. An

animation of the data helped interpret the results. It was found that the instantaneous position of the turbine had little effect on fluid flow inside the impeller passage. The turbine did, however, have noticeable effects on the flow in the gap region. It was also recommended that the LDV system be upgraded to be able to measure all three velocity components simultaneously. This would better provide information necessary to understand actual three-dimensional fluid flow.

It is important to point out here that a 5-beam probe was purchased for the purpose of measuring all three components simultaneously, as recommended. After much time and effort it was determined that measuring three components simultaneously was not a realistic option at this time. Instead, efforts were then put in to mapping the flow fields in one and two dimensions. Pertinent details shall be covered in Chapter 4.

CHAPTER 2

EXPERIMENTAL EQUIPMENT

2.1 Test Facility: Test Rig

The test rig assembly consists of a torque converter fixture, a bedplate, a 50 Hp DC drive motor and a 50 Hp Universal Dynamometer (Figure 2). The converter fixture supports the modified torque converter assembly and allows optical access into the converters for flow studies. The bedplate is used to support the fixture assembly with a fixture bracket. Located below the bedplate, used to drive the converter assembly, are a 50 Hp DC drive motor and a 50 Hp Universal Dynamometer, which has an eddy current dynamometer motoring feature. The 50 Hp DC drive motor is used to simulate an automotive engine, whereas the 50 Hp Universal Dynamometer simulates load conditions. A belt drive mechanism is used to couple the motor, dynamometer and torque converter fixture.

The DC drive motor can produce a maximum of 2500 rpm, and is geared at a 2:1 ratio to that of the torque converter pump (impeller), resulting in a converter speed of 5000 rpm. The Universal Dynamometer is at a 1:1 ratio and drives the converter (turbine) at 5000 rpm. The

speeds of the motors are controlled independently through the use of separate controllers.

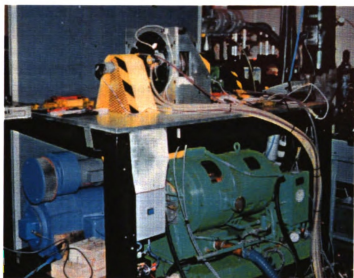


Figure 2. View of Test Rig

2.2 Transmission Oil Supply System

The transmission oil supply system controls pressure, flow rates, and temperature (Figure 3). The transmission oil supply system is divided up into two separate systems. One system is used to supply transmission oil to the torque converter, charging the impeller, turbine, and stator passages. The other system supplies lubrication oil to the support bearings, which support the torque converter assembly. The pressures and flow rates are controlled for each system with the use of regulators and are monitored through the test rig controller. The bearing lubrication oil

is filtered and is used in conjunction with a vacuum pump to ensure efficient flow through the bearings.

The temperature of the transmission oil is controlled through the use of a water-cooled heat exchanger. This ensures the necessary temperatures for operating conditions during testing. The transmission oil is measured using type T thermocouples enabling the monitoring of the oil as it both enters and leaves the converter assembly. Another important use of the supply system is that it controls particle distribution in the transmission oil. Proper particle distribution is necessary for consistent flow and laser velocimetry measurements.



Figure 3. Transmission Oil Supply System

2.3 Test Rig Controller

The test rig controller operates and monitors the test rig assembly and the transmission oil supply system. The controls consist of both hard wired and computer controlled switches with a complete readout of the systems functions. LabVIEW is the software used in the test rig controller for the readout (Figure 4).

The test rig controller measures torque on the shafts of the impeller, turbine and stator through strain gauges. It also measures oil temperatures, pressures, and oil flow rates. It maintains constant speed and torque controls, as well as, records all measured parameters. Figure 5 shows the test rig and test rig controller.

2.4 LDV System

The LDV system is capable of measuring inside complex geometries such as the automotive torque converter (Figure 6). The components used in this LDV measurement system are an Argon-ion laser, a ColorBurst (TSI), a 4-Beam Fiberoptic probe, a digital burst correlator (TSI, IFA 750), a traverse mechanism (TSI, Model 9900-1), and a personal computer (PC). LDV measures fluid velocities by detecting the Doppler shift frequency of the laser light that has been scattered by small particles (~10 μm) flowing within the fluid at the same velocity as the fluid flow. These

particles are metallic coated plastic for efficient light scattering qualities. When two beams cross a fringe pattern is formed (Figure 7). Particles pass through this fringe pattern and the light is scattered. The scattered light is collected by a photomultiplier detector and converted into voltage signals.



Figure 4. VI Screen Display

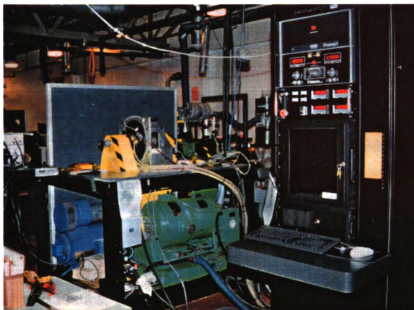


Figure 5. Test Rig and Test Rig Controller

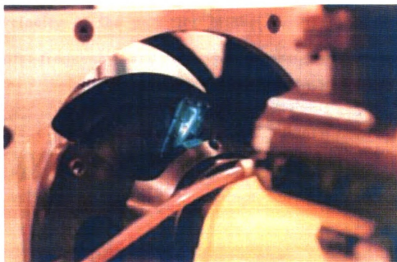


Figure 6. View of 4-beam probe of LDV system and test rig with front window converter

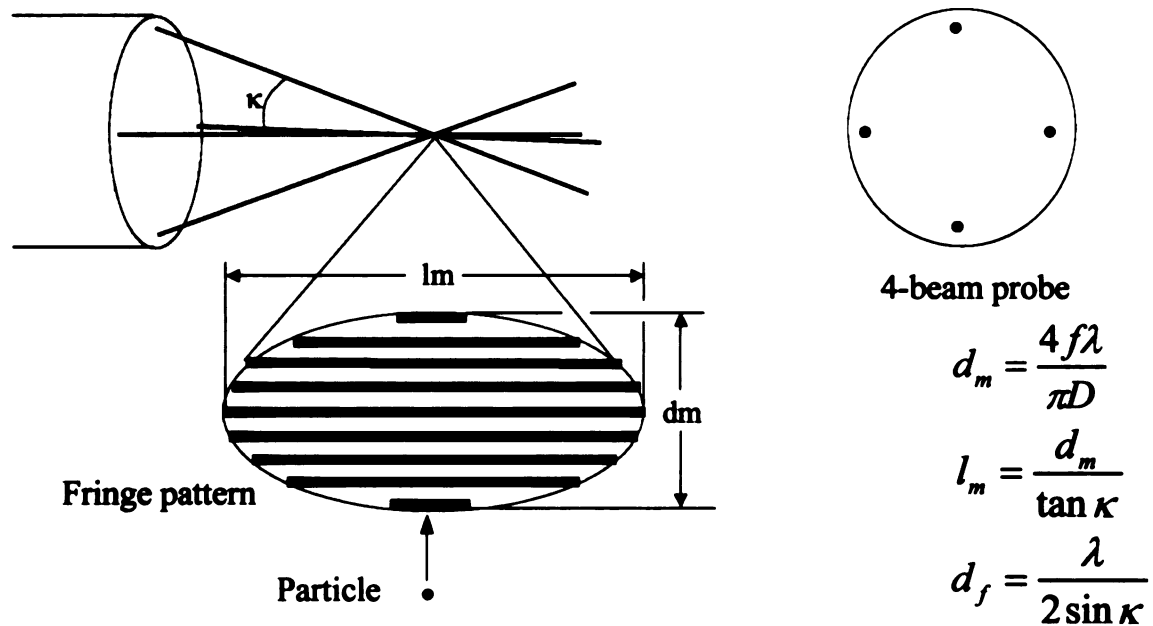


Figure 7. 4-beam probe with fringe pattern

The velocity of the particles in the fluid is proportional to the Doppler shift frequency and can be determined by the following relationship:

$$Vel = d_f / t_1 = d_f \times F \quad (2.1)$$

where

d_f = fringe spacing

t_1 = time taken for the particle to cross a pair of fringes

F = Doppler shift frequency of the scattered light

The fringe spacing, d_f , can be readily determined by:

$$d_f = \lambda / (2 \sin \kappa) \quad (2.2)$$

where

λ = wavelength of the laser light

κ = half angle between the beams

The Doppler shift frequency, F , is measured in hertz and is equal to the number of fringe patterns a particle crosses in one unit of time. The frequency shifter allows flow reversals to be measured. A multi-wavelength laser beam from an Argon-ion laser is separated by the ColorBurst into green, blue, and violet beams. The Digital Burst Correlator (IFA 750) distinguishes the burst signal from the noise. The IFA 750 analyzes the Doppler signals so that the velocity components at the measured position can be calculated in coincidence mode. These transmitting beams are linked to the fiberoptic probe through fibers that connect to the fiber coupler on the ColorBurst.

A 4-beam fiberoptic probe was employed to measure one or two velocity components. The function of the 4-beam fiberoptic probe is to transmit the laser beams to form the measurement volume and to collect the light scattered by the particles traveling in the measurement volume. Single-mode polarization-preserving fibers carry the green, blue, and

violet beams to the probe. The diverging cone of light emitted from each fiber is focused at the measurement volume with a lens. For this study both green and blue beams were utilized depending upon components measured. In the measurement volume, constructive and destructive interference forms the pattern of dark and bright fringes.

The 4 beams consist of two pairs of single wavelength beams, which are green (514.5nm), and blue (488nm) beams. A fifth fiber, known as the receiving fiber, is used to collect the light scattered by the particles as they pass through the fringe spacing. This method used is known as the on-axis backscatter method. Off-axis forwardscatter is more efficient, however due to the complicated nature of the optical access to the torque converter, this method could not be used.

In this study, a pair of blue beams are located vertically, while the green beams are aligned horizontally. The 4-beam probe is used to measure the horizontal and vertical velocity components perpendicular to the optic axis.

CHAPTER 3

TORQUE CONVERTER

3.1 Modification

Two Ford Motor Company production torque converters of the same design were modified for optical access for internal flow measurements. One converter required optical access into the lower impeller passage up through the impeller exit (front window) and the second for access at the impeller-turbine interface (side window). Table 1 shows the specifications of the production torque converter used. There were two parameters that needed to be addressed during the modification process. The first, installation of the window must not interfere with the fluid flow inside of the torque converter during operation. Doing so would greatly reduce the accuracy of the results. Second, the window must allow a clear access for the beams to pass through into the converter when measuring.

The production torque converter was modified at Ford by cutting the converter in half radially and welding mild steel flanges to each section of the converter. Holes were drilled and tapped in the flange and bolts inserted to hold the assembly together. This modification allowed for quick access to the components inside of the torque converter for easy alterations and reassembly (Figure 8).

Table 1. Ford production torque converter specifications

Torque Converter Specifications	
Diameter (mm)	267
Axial length (mm)	95.5
No. of Impeller blades	31
No. of Turbine blades	27



Figure 8. View of impeller half of converter with front window installed

3.2 Front Window

For the front window installation a section of the impeller passage was milled. This included an area from approximately mid-way up the impeller passage to the impeller exit. This allowed for optical access to the impeller passage, gap region, and turbine passage. An acrylic Plexiglas was chosen as a window material since its refractive index was close to that of the transmission oil used. The inside surface of the window follows the curvature of the inside surface of the converter housing, so that fluid flow inside the converter should not be disturbed (Figure 9). Another property to consider was temperature. The internal converter temperature must be maintained below the point at which the Plexiglas will lose strength and possibly deform.

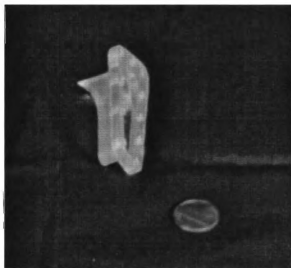


Figure 9. View of front window

3.3 Side Window

For the side window the modification was similar to that of the front window. The flange was installed in the same manner as the front window for quick access for easy alterations as needed. Plexiglas was also used as the material for the side window for the same reasons as the front window. The side window was installed to gain optical access to the impeller passage, the gap region, and the turbine from a different perspective (Figure 10). This location allowed for data to be measured in 1-D flow from the impeller passage out into the gap region to the turbine. This data would provide a third component to the fluid flow measured.

One area of concern was the geometrical requirement of the side window to follow the inside curvature of the converter. In this location on the converter the side windows inside surface was much more contoured as compared to that of the front window. When measuring, the beams pass through the window and the focal point is inside the converter. If there is refraction of the beams when they pass through the window then the true location of the focal point may not be known. This issue is addressed in detail in chapter 4.



Figure 10. View of impeller half of converter with side window installed

CHAPTER 4

EXPERIMENTAL PROCEDURE

4.1 Preliminary Testing

As mentioned in the introduction, a 5-beam probe was purchased from TSI. This device offered the promise of a three-component measurement through a single focusing and collecting lens. It operates under similar conditions as the 4-beam probe in terms of setup and operation. This was a TSI model 9233 fiberoptic 5-beam probe capable of measuring three velocity components simultaneously. One concern, when used for this project, was the obtainable data rate for all three pairs of beams in coincidence mode and another was the beam half angle used relative to the accuracy of the data acquired. After careful calibrating, testing, and measuring it was determined that the 4-beam probe was best suited for this study over the 5-beam probe.

4.2 Setup

Periodic maintenance was performed such as the transmission oil changes because of oil oxidation, and its effect on signal degradation through optical absorption. Once the converter assembly was installed

and the system was ready, a number of steps were performed via the following checklist.

1. The traverse table zero point is set so that the coordinate system origin is known.
2. The impeller and turbine zero reference points are set for the shaft encoders.
3. The beams focal point is moved inside the converter through the window.
4. Frequency shifters and receiving optics are set and adjusted.
5. The chosen speed ratio is set.
6. The system, such as temperature, pressure, and flow rates are allowed to stabilize.
7. The data rate and quality are checked.
8. The data acquisition software (TSI Phase) is programmed.
9. Data is acquired and recorded.

The traverse table must be referenced to the torque converter assembly when moving the focal point to necessary locations to be measured (Figure 11). The traverse table moves in three-dimensional Cartesian coordinates and referencing is accomplished through the use of the LDV laser beams.

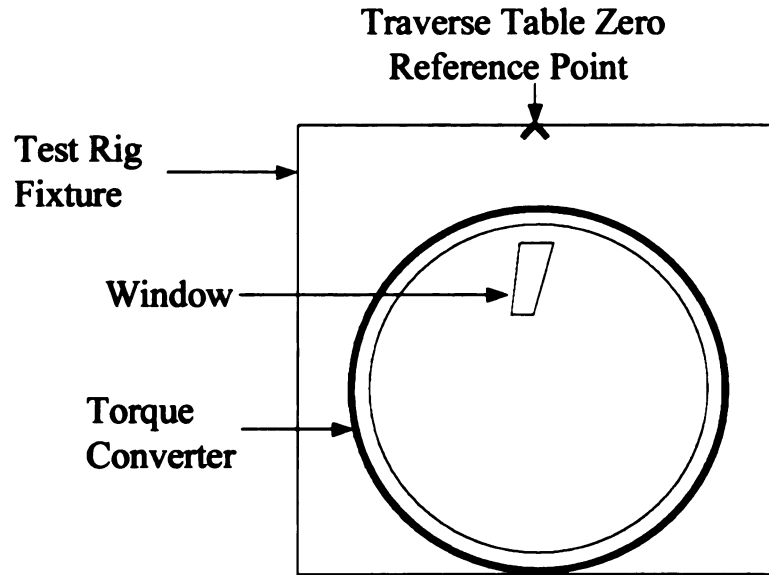


Figure 11. View of test rig apparatus for traverse table reference point

The encoder zero degree reference points are set by use of the LDV laser beams, angle encoders and also a Tektronix 2445 oscilloscope (Figure 12). For the impeller the welding tab on the shell of the converter of the following impeller blade is used, whereas, for the turbine the surface of the turbine blade itself is used. Once the beams are oriented the shaft encoder trigger signal is viewed on the oscilloscope and the encoder is then set.

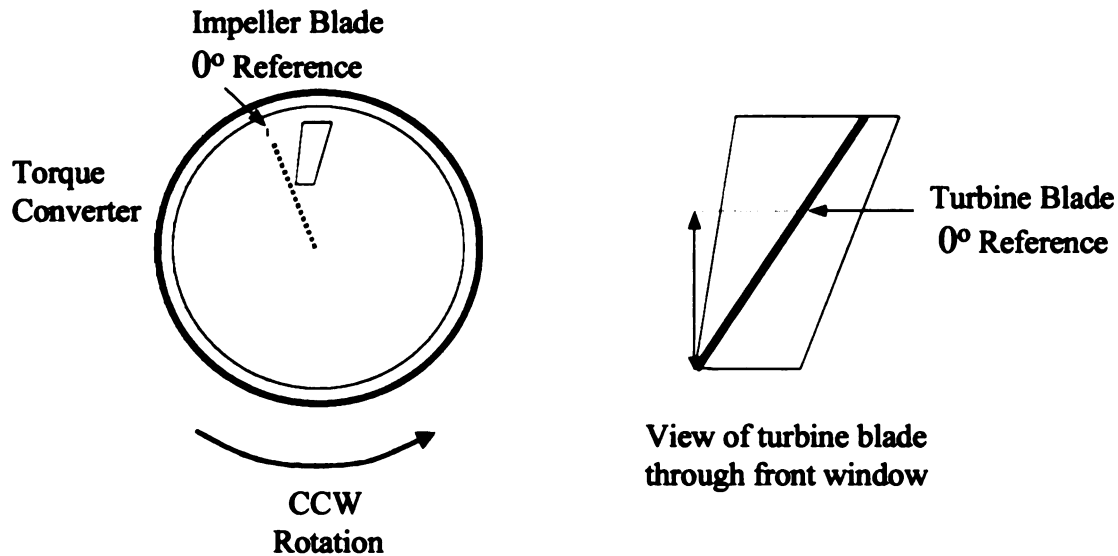


Figure 12. View of Impeller and Turbine positions for encoder references

4.3 Data Acquisition

The internal flows in the torque converter were quantified using the 2-D LDV system previously described. The data measured totaled three different data series. The first and second series were measured through the front window, while the third series was measured through the side window. A total of 9 planes were measured, 5 through the front, and 4 through the side window. All three data series were measured at two speed ratios. The first being a speed ratio of 0.4, with an impeller speed of 1600 rpm and a turbine speed of 633 rpm and the second speed ratio is 0.8, with the impeller speed of 2000 rpm and a turbine speed of 1600 rpm. Coordinates from Ford blueprints were used to generate wire frames of

of

3)

na

he

he

on

ve

on

the

no

ot

vic

on

pr

th

th

bi

th

Th

both the impeller and turbine in the computer animation series (Figure 13). The LDV's Cartesian coordinate system has been transformed to match Ford's coordinate system (FCS) for convenience. Therefore all of the results shown will be in FCS.

The blue and green arrows in Figure 13 represent the beams from the LDV system as they travel through the front window into the converter along the positive y-axis. For the front window series there were 2-D components measured. In the side window series there was 1-D component measured, which was done to provide toroidal flow characteristics. The locations of the vector components for both the front and side window series are shown (Figure 14).

The views are side views of the impeller and turbine and the rotation of both rotors is counter-clockwise (CCW). The CCW rotation is viewed from the left side of the LDV beam perspective, therefore the rotors rotate into the page at the top of the view (hence the suction and pressure side of the impeller blade).

The vectors represented in Figure 14 are an example of a point of the plane measured. For the front window the LDV beams enter through the window from the left and measure the two components shown. The blue beam is the vertical component (positive z direction) measured and the green beam represents the horizontal component (positive x direction). The side window has the LDV beam entering through the window at the

top of the assembly for one component measurement. Here the green beam indicates the toriodal flow measured (positive y direction).

9 planes were measured at different locations within the converter (Table 2). The z and y-axes are listed without the x-axis. This is because the planes (z and y-axes) represent the total area measured and the x-axis location represents the point measured in each plane. The point measured varies due to rotation because the measurement was based on cylindrical coordinate system and was conducted through a circumferential line. Therefore, the circular line can be defined by two coordinates such as y (for depth) and z (radius). The arrows indicate the direction in which the data were measured.

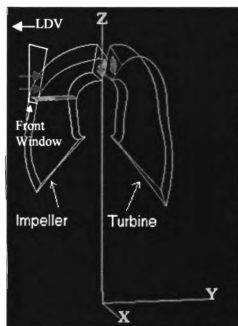


Figure 13. View of impeller and turbine blades inside the torque converter with measured planes (Ford coordinate system)

Table 2. Measured plane locations in Ford coordinate system

Data Measured	Location (mm)	
Front Window	Y	Z (radius)
Plane 1	-30.42→-11.78	93
Plane 2	-2.09	105→112.5
Plane 3	3.88	105.5→112
Plane 4	-2.09	105→112.5
Plane 5	-0.43	105→111
Side Window		
Plane 6	-5.41	112→107.5
Plane 7	-4.42	113.5→108
Plane 8	-2.29	117.3→103
Plane 9	-1.29	117.8→112

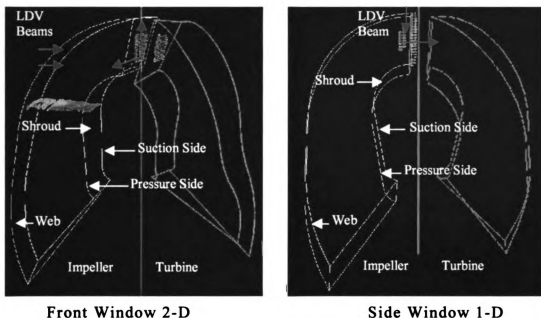


Figure 14. Views of measured vector components in both front and side window series

The LDV system, including the 4-beam probe, rests on a TSI model 9900-1 traverse table that is capable of moving in a 3-D Cartesian coordinate system within an accuracy of $\pm 1.0\mu\text{m}$. The 4-beam probe is positioned for measurement locations as necessary.

When data is being measured the data acquisition system collects the raw velocity and angular position of impeller and turbine information. This is done using the output of two rotating machinery resolvers (RMR), IFA 750, and TSI software known as Phase. Flow data was collected based on the impeller and turbine angles, which were detected by an angle shaft encoder installed on each rotor. Each encoder generates one square pulse per revolution (OPR) and two series of 1024 square pulses per revolution. A total of 4096 pulses per revolution were used. The RMR's

(one for each rotor) record the angle from the encoders and attach it to the velocity measured. These measured angles are then passed to the IFA 750, which collects the data in bins and stores it in the PC. The TSI Phase software monitors parameters such as the data rate, measurement time, as well as calculating velocities from frequency information.

During the experiments, the equipment was allowed to run for at least 30 minutes to be sure pressures and temperatures had stabilized. Preliminary checks are made in association with the data rate to be sure criteria such as proper particle distribution is correct. Test conditions utilized for both speed ratios were supplied by Ford and are based on normal operating conditions of the torque converter (Table 3).

Table 3. Test conditions for data measured

Speed Ratio 0.4				Speed Ratio 0.8			
Oil Temp (°C)		Pressure (PsiG)		Oil Temp (°C)		Pressure (PsiG)	
Vent	40	Vent	75.62	Vent	30	Vent	76.16
Charge	40	Charge	59.83	Charge	30	Charge	65.16
Discharge	65	Discharge	35.86	Discharge	50	Discharge	36.79

4.4 Measurements with Front Window: First Series

There are three planes where two component velocity vectors were measured in series 1 (Figure 15). The blue beam pair was used to measure the vertical component measured along the positive z-axis, and the green beam pair was used to measure the horizontal component along the positive x-axis for all three of the planes (FCS). Ford determined the plane locations that were to be measured. The first plane was measured mid-chord in the impeller passage. This plane starts at the web side of the impeller passage and continues along the positive y-axis (FCS), with the plane extending toward the z-axis, to the shroud side (plane 1, Figure 15). The purpose of making measurements in this plane was to study the uniformity of the flow as it continues toward the impeller exit.

The second plane was measured at the exit of the impeller passage. This plane begins at the shroud side (at the bottom of the impeller exit), extending along the positive z-axis to the web side at the top of the impeller exit (plane 2, Figure 15). The purpose of making measurements this plane was to study the fluid flow as it continues from the impeller exit out into the gap region.

The third plane was measured approximately 1mm inside the turbine passage. This plane begins at the shroud side (at the bottom of the turbine inlet), extending along the positive z-axis to the web side at the

top of the turbine (plane 3, Figure 15). Velocities in the third plane were measured to map the fluid flow as it entered the turbine.

4.5 Measurements with Front Window: Second Series

For the second series two planes were measured in two components, where the blue beam was the vertical component measured along the positive z-axis, and the green beam being the horizontal component along the positive x-axis (Figure 16). Plane 4 is located at the impeller exit with the plane extending along the positive z-axis. This area was chosen to map fluid flow characteristics as the flow leaves the impeller passage.

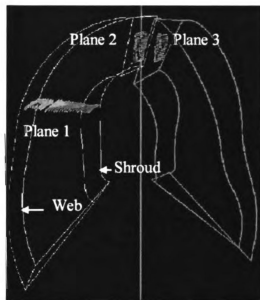


Figure 15. First Series with 3 planes

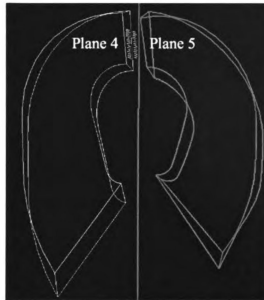


Figure 16. Second series with 2 planes

Plane 5 was measured 1mm past the impeller passage into the gap region, also extending along the z-axis. This area was measured to map flow characteristics as the fluid leaves the impeller passage and enters into the gap region.

4.6 Measurements with Side Window: Third Series

For this data series the torque converter with the front window was removed from the dynamometer test stand and replaced with the torque converter with the side window. There are four planes where one component flow was measured from the top of the torque converter (Figure 17).

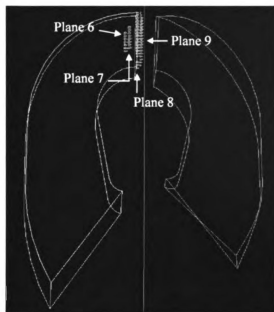


Figure 17. Third series with 4 planes

This was to represent the 3rd component of the fluid flow (in the y-axis direction) allowing for additional information of the trends observed measured through the front window. Four parallel planes in this region were studied. Plane 6 is inside the impeller passage 2mm from the exit and extends along the positive z-axis. Plane 7 is inside the impeller passage 1mm from the exit also along the z-axis. Plane 8 is at the impeller exit and plane 9 that is 1mm outside the impeller passage in the gap region. Two of the planes (planes 8 and 9) are close to the location of the front window measurement series (planes 2,4 and 5).

4.7 Side Window Geometry

One area of concern was refraction and reflection associated with the non-linear curvature of the side window lens. While it is imperative that the lens matches the inside geometry of the torque converter (else fluid flow would be altered), it is equally important that the location of the focal point be known when actual measurement takes place. Much effort was put into determining the curvature of the lens therein by locating the focal point at given intervals along its inside surface (Figure 18).

One point of particular concern was the sharp curvature at the exit plane of the impeller. The question posed was, is the focal point truly at the measured location believed, or had it moved based on the refraction effect on the laser beams as they left the lens?

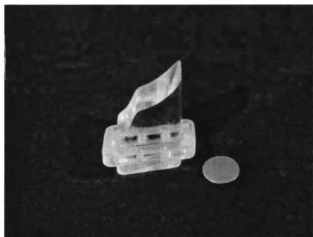


Figure 18. View of side window

A Plexiglas box was constructed with the side window lens installed in its side and the box was then filled with base stock transmission oil. The LDV system was then used to determine the location of the focal point as it moved along the lens surface (Figure 19). The result showed a good approximation of the focal point as it moved however; it was not accurate enough to be sure of the actual distance the focal point varied. Other methods were attempted, such as video taping and photographing the focal point in the torque converter at measured locations, however the resolution was still poor.

The next step was to have the lens surface carefully measured which would enable a more exact location of the focal point to be calculated. Demmer Corporation, with the use of a coordinate-measuring machine (CMM), measured the lens and mapped the points to an accuracy of $1.0\mu\text{m}$. Particular emphasis was placed on the curved areas of the lens. The result received from Demmer was in an IGS file format that was then used as a database for a c-spline surface representation, which was implemented in a computer code (Figure 20). Using this code, the focal intersection of the laser beams measured locations was calculated. Variations were found to be less than 0.2mm of the overall movement of the focal point for the range of measurement for this study. This was believed to be the most accurate way to determine the focal point location. It was found that where the actual measuring took place the focal point was not far enough beyond the surface of the lens

(approximately 5.0mm) to make a significant difference in spatial location.

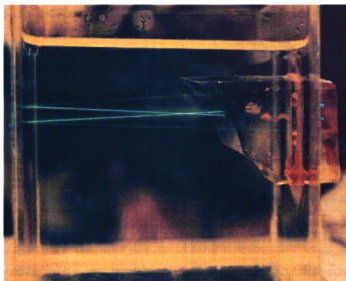


Figure 19. View of beam focal point through the side window

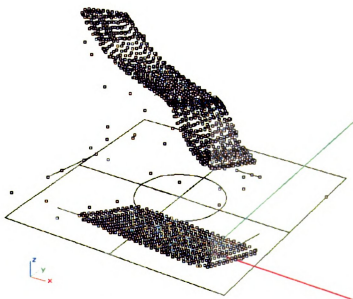


Figure 20. 3-D display of side window (Demmer)

4.8 Data Post Processing

Post processing of the LDV collected data involves many different aspects. The data collection process is shown (Figure 21). The test rig controller, which is used to record the strain, pressure, and temperature during testing and this information is then stored in a file. The test rig controller also determines the speed, torque, etc. of the test rig. Sensor feedback occurs from the test rig to the test rig controller. The receiving optics (located inside of the 4-beam probe) collects the scattered light and is changed to voltage signals by the photomultipliers. At the same time the RMR's are attaching an angle, based on encoder information to each velocity component measured. The RMR's pass this information to the IFA750. The frequency shifters control the frequency and direction (usually against the mean flow) of the data rate via the Bragg cell and this information is sent to the IFA750 as well. The IFA750 stores all of the information into bins and then relays this information to the PC to be stored. The PC sets the IFA750's details through the Phase software at the onset of the testing. This process continues one spatial point at a time until a data set for one location is measured. Then the traverse table is used to move the focal point from one location to another location to be measured and the process begins again and is repeated until a full plane is mapped. It is important to mention that each point measured must

generate a line of data due to the converters rotation, thus as each point is moved a plane is the result.

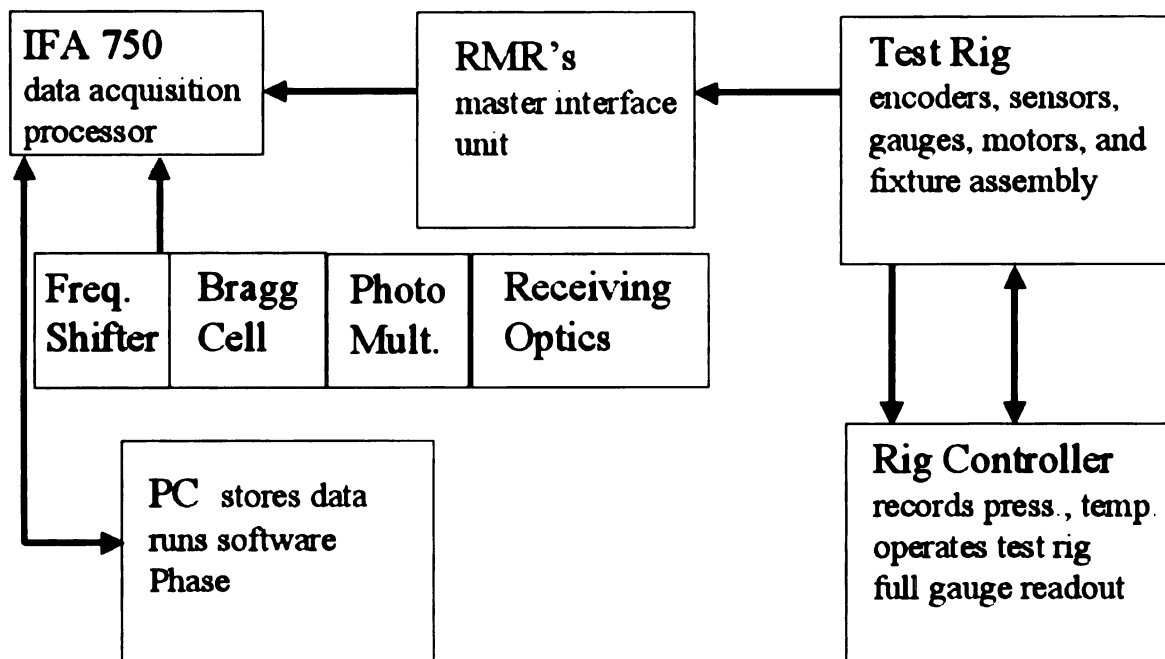


Figure 21. Data acquisition flow chart

At this point the measured data is ready for processing. For the torque converter LDV data is collected through an area the same width of the impeller passage. The shaft encoders allow for the instantaneous positions of both the impeller and turbine to be recorded each time a velocity measurement is acquired by the system. The data stored in the PC is in the form of raw data (Figure 22). The raw data file is in binary format and contains information such as the measured velocity, magnitude, encoder values, and cycle number in the frequency frame of reference.

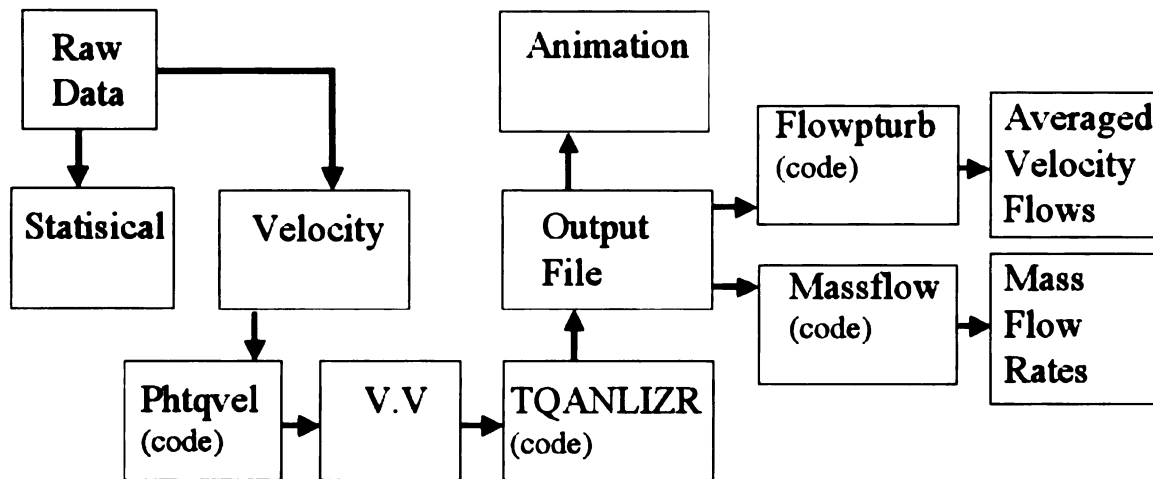


Figure 22. Data processing flow chart

The cycle number is relevant in that the data is measured over time, which is necessary for data accumulation. Therefore, there is no cycle-to-cycle variation present in the data.

The raw data file can be processed through Phase, changing the format from binary to ASCII and produces two output files known as statistical and velocity. The statistical file contains information such as standard deviation, number of points collected, and velocity mean, among other data. One primary advantage of the statistical file is that it plots the data in angle of degrees versus the points measured. This provides a quick indication to see if the data recently measured is correct.

The velocity file contains the necessary information for processing, however it is not in the correct frame of reference needed. The TSI code Phtqvel basically changes the frame of reference in the velocity file from the frequency domain to the time domain, with the output file called the

V.V file. This TSI code Phtqvel was modified to handle large files consecutively. The output file (V.V) can now be processed into the format necessary for animation.

A FORTRAN code called TQANLIZR was written to produce an output file in the format required by Ford engineers for comparison with simulation results and for animation. TQANLIZR is used to sort the data into bins containing information, such as velocity and encoder angles for the impeller and turbine through ensemble averaging. The data is collected in bins of 0.5° from the respective angular positions. This bin number was chosen to generate a uniform grid suitable for animation. Since the turbine and impeller rotate at different speeds and the measurements are made through an impeller window; the turbine can be any place within the window at any given moment in time, hence the turbine angular measurement range is 360° of rotation. For that reason at each impeller angle all of the turbine angles are simultaneously recorded. All turbine angle measurements are approximately 0° to 13.3° . The impeller angle value ranges from 0° to approximately 11.6° coinciding with the width of the window in the impeller side of the converter. An additional consideration is to ensure that the impeller and turbine angles are represented from the same perspective since each is measured independently. This allows for the animation to represent the passing of the turbine blade with respect to the impeller blade angles recorded.

TQANLIZR is also used for coordinate transformation. The data is collected initially in Cartesian coordinates with respect to the LDV system axis and is then stored in terms of cylindrical coordinates. The data is then transferred from the initial coordinate system to the Ford coordinate system in cylindrical coordinates and grouped into bins. The fact that the code transfers the coordinates from the MSU LDV coordinate system to the Ford coordinates for animation adds credibility to the accuracy of the location of the measured planes. That is, rather than just place the velocity profile results in locations in the Ford coordinate system for animation purposes manually, the code uses the LDV coordinates inputted and transfers the coordinate system into the FCS, placing the data in the proper locations. The data also is converted into the impeller frame of reference for when viewing the animation series. For animation the SGI software explorer coordinate system was set up to match Ford's coordinate system.

The process for the side window data is similar to that of the front window. TQANLIZR was modified for the side window to incorporate the cubic spline code accounting for window curvature. The front window was used to gather two component data, whereas the side window was used to gather one component data for the toroidal flow near the impeller exit and the gap region near the turbine entrance. This data is gathered from different perspectives and uses two unique windows for viewing the flows. TQANLIZR then generates an output file that can be read by the

SGI animation software. As with the front window the data information, measured in the side window is converted into the impeller frame of reference in order to facilitate the animation process.

When viewing the animation, data is presented frame by frame over all of the turbine angles. The results section show significant aspects of these animations. These snapshots were chosen because they show distinct flow characteristics noted in the animation, however the average flow rate is only of that particular frame. A second code was written to provide more information that could be derived from the output files from TQANLIZR. The Flowpturb code produced an output file containing the average flow of the entire measured series for each plane in one frame. Each series was then animated. The turbine is not included in the animation since the vectors shown are the results of all the turbine angles for each impeller angle measured. Since the velocities are averaged for each impeller angle, the turbine would appear as a solid passage. The advantage here is the average flow rate in meters per second can be estimated and used to gain a perspective of the overall fluid flow measured. The disadvantage is distinct flow characteristics, such as blade-passing effects cannot be clearly seen.

For purposes of assisting the computational fluid dynamics (CFD) code development, the code Massflow was written to show the mass flow of the fluid normal to each plane measured. Here all of the turbine angles were ensemble averaged at each measured impeller position. The output

file contains the position, as well as, the mass flow rate in kg/s. This result would show the primary characteristics of the toroidal flow and can be used for flow comparison of experimental results with those of the CFD results. Not all of the planes measured fit these criteria. The vertical component for plane 1 was useful for the primary mid-chord flow of the impeller passage, which was measured in the front window series. Planes 6-9 provided primary flow characteristics measured in the side window series. Planes 2-5 were not used since the components measured provided secondary flow information.

4.9 Animation

The velocity profile animation series was processed through the use of an SGI workstation and EXPLORER software. There are several details about the animation that need to be addressed. First, the animation provides a view of the final results, after the data has been processed from the output files containing coordinates and velocities of each plane measured. Second, the animation is constructed with the impeller used as the reference frame. More specifically, the observer views the results from the perspective of sitting on the impeller and watching the relative fluid flow and turbine motion. Third, the figures shown in the results and discussion of this report are single frames taken from the animation series and were chosen to show the observer important fluid flow characteristics.

These snapshots provide particular details about flow characteristics in each plane observed during the animation. A complete animation is available in high 8 and VHS format as part of this work.

CHAPTER 5

RESULTS AND DISCUSSION

5.1 Measurements with Front Window: First Series (Planes 1-3)

When viewing these Figures, the planes are rotated to an optimal position to best display the results. The picture on the lower right-hand corner of the Figure shows the planes measured location. The green and white arrows correspond to the measured and view perspectives, respectively. The white wire frame generated represents the impeller and the red wire frame, the turbine. Cartesian coordinates are also provided to assist in plane orientation when viewing these Figures. All of the planes are rotated CW on the z-axis, with a small number (of Figures) tilted slightly for additional data clarity. The upper half of the figure is a picture that shows the details of the planes flow pattern characteristics mapped.

The results are discussed by dividing the measured planes into sections. The first section discusses the plane results for the 0.8 speed ratio. The second discusses the 0.4 speed ratio and the third discusses comparisons of both speed ratios. Subsequently there is discussion of comparison of particular planes for both the front and side window series.

5.1.1 Plane 1: 0.8 Speed Ratio

Plane 1 was measured mid-chord of the impeller passage. The flow pattern for the 0.8 series was similar to that of the 0.4 speed ratio (Figure 23). The measured velocities were slightly lower for the 0.8 speed ratio case, at an average velocity of 8.5m/s, as opposed to 9.2m/s in the 0.4 case. Here the vectors vertical component (positive z direction) was not generally uniform from the suction side to the pressure side of the passage. Rather, the flow pattern increased in magnitude (positive z and x direction) as it approached the pressure side of the impeller passage. Numazawa had similar results for vector magnitudes from the suction side to the pressure side of the impeller passage [20]. The flow at the shroud side of the impeller passage was smaller in magnitude. This flow pattern also moved in a different direction than that of the rest of the plane (positive x and -z direction), with vectors pointing downward (-z), or straight across (+x), as it moved from the suction to the pressure side of the passage.

5.1.2 Plane 1: 0.4 Speed Ratio

The vertical component (+z direction) was generally uniform from the suction side to the pressure side of the impeller passage (Figure 24). The average velocity of the fluid flow was 9.2m/s. The fluid flow

generated in the animation showed a general uniform trend (+z and +x direction) along the impeller passage, with the exception of an area at the shroud side of the passage. At the shroud side of the passage, a band of flow smaller in magnitude was observed. This band of flow traveled downward (-z direction) as it moved to the pressure side from the suction side of the impeller.

5.1.3 Plane 1: Comparison of Both Speed Ratios

Plane 1 was measured mid-chord of the impeller passage (Figures 23 and 24). For both speed ratios the data was processed and animated. There were no noticeable turbine blade-passing effects in the flow at this location. This result is consistent with the findings of McCarrick [21]. The general trend of the fluid flow traveled upward towards the impeller exit, with the direction of the vector magnitudes from the suction side to the pressure side of the impeller (positive x direction). This flow pattern included the whole plane with the exception of a small area near the shroud side of the passage. At the shroud side of the impeller passage, a band of flow smaller in magnitude was found. This flow also moved in a different direction (positive x and -z direction) than that of the rest of the plane [21]. This could result by flow from behind the core ring re-entering the impeller passage through the blade tab slots. Another

possible explanation is that due to the geometry of the shroud a type of shear flow may be occurring. Further studies are necessary to be certain.

5.1.4 Plane 2: 0.8 Speed Ratio

Plane 2 was measured at the impeller exit. The flow pattern moved in a general uniform direction (+x direction) from the suction side of the impeller passage to the pressure side (Figure 25). The average velocity of the fluid flow was 5.5m/s. The flow magnitudes increased (+x direction) from the suction to the pressure side as in the previous case. As the flow moved across the passage, the vector angle (from horizontal to vertical) was generally increasing as the flow continued to the pressure side. There were some steeper velocity gradients observed along the bottom of the plane.

5.1.5 Plane 2: 0.4 Speed Ratio

The flow pattern moved in a general uniform direction (+x) from the suction side of the impeller passage to the pressure side, however this flow contained steeper velocity gradients than in the 0.8 speed ratio case (Figure 26). The average velocity of the fluid flow was 3.3m/s. As the flow moved from the suction side to the pressure side of the impeller passage, the flow magnitudes were not at a generally increasing angle

(horizontal to vertical) as with the 0.8 speed ratio case. Instead, the overall flow pattern moved up (+z direction), then down (-z direction), in a type of s-curve, as it continued toward the pressure side. There were also steeper velocity gradients observed along the lower portion of the plane.

5.1.6 Plane 2: Comparison of Both Speed Ratios

Plane 2 was measured at the impeller exit (Figures 25 and 26). For both speed ratios the data was processed and animated. Here the general flow pattern of the fluid traveled out of the impeller exit, with the direction of the flow magnitudes (+x direction) from the suction side to the pressure side of the impeller. The magnitudes of the flow were smaller on the suction side of the impeller passage than that of the pressure side for both speed ratios. This would be expected due to the rotation of the torque converter.

Blade-passing effects of the turbine were found, although this effect was more prominent at the 0.4 speed ratio than at the 0.8 speed ratio. McCarrick found this effect in the gap region, however not as far back as the impeller exit [21]. As the turbine blade passed in front of the impeller passage the velocity of the flow field was affected. The blade-passing effect appears to trail the actual turbine blade, which indicates a time delay between the turbine blade and the measured plane. This may be

caused by a ripple effect from the fluid created from the turbine blade as it passes. This ripple effect propagates along the gap region back to the impeller passage. The animation generated for this series clearly shows this effect.

5.1.7 Plane 3: 0.8 Speed Ratio

Plane 3 was measured 1mm into the turbine passage. The average velocity of the measured flow field was 6.5m/s (Figure 27). The magnitudes of the vectors on the pressure side of the turbine were fairly constant (+z and x direction), with the exception of some higher velocities at the bottom of the plane near the blade. On the suction side of the turbine, the vector magnitudes varied somewhat more than on the pressure side. Steeper velocity gradients were observed along the top of the plane.

5.1.8 Plane 3: 0.4 Speed Ratio

The magnitudes of the flow on both the pressure and suction side of the turbine varied more than in the 0.8 speed ratio case (Figure 28). The average velocity was 7.2m/s. Steeper velocity gradients were observed along the edge of the suction side of the turbine and along the bottom of the pressure side. On the upper left-hand region there is a band of blue vectors moving upward (+z and x direction) at a speed of 6.0m/s.

5.1.9 Plane 3: Comparison of Both Speed Ratios

Plane 3 was measured 1mm into the turbine passage. This plane showed a distinct band with no data that directly correlates to the turbine blade as it passes (Figures 27 and 28). This is clearly evident in the animation. Since this data was measured approximately 1mm in the turbine passage the band is the from the actual turbine blade itself. The overall velocity of the fluid was also slowing down, which is expected since the fluid is now doing work on the turbine blade. The fluid flow field impacts on the pressure side of the turbine blade causing the turbine to rotate. On the suction side of the turbine the flow appears to follow the blade (+z and x direction).

5.2 Measurements with Front Window: Second Series (Planes 4 and 5)

5.2.1 Plane 4: 0.8 Speed Ratio

Plane 4 was measured at the impeller exit. The flow pattern showed general flow direction from the suction side of the impeller passage to the pressure side (Figure 29). The average velocity of the fluid flow was 3.0m/s. The flow magnitudes increased (+z and x direction) from the suction to the pressure side, with the exception of along the bottom of the plane where the flow moves in the -z and +x direction. For

the upper half of the plane the fluid flow moved across the impeller passage, where the vector angle was generally increasing (horizontally and vertically) as the flow continued to the pressure side. For the bottom half of the plane the flow moved straight across (+x) or even downward (-z) as it approached the pressure side. There were steeper velocity gradients also observed along the bottom of the plane.

5.2.2 Plane 4: 0.4 Speed Ratio

The flow pattern is shown in Figure 30. This flow magnitudes varied more than in the 0.8 speed ratio case. The average velocity of the fluid flow was 5.5m/s. As the fluid flow moved from the suction side to the pressure side (+x direction), the flow does not have the same general increasing angle (+z and x direction) as with the upper half of the 0.8 speed ratio case. Instead, for the majority of the plane the flow direction moved downward (-z) as it continued toward the pressure side. A larger portion along the bottom of the impeller passage also included steeper velocity gradients.

5.2.3 Plane 4: Comparison of Both Speed Ratios

Plane 4 was measured at the impeller exit (Figures 29 and 30). Blade-passing effects of the turbine were found in both the 0.4 and 0.8

speed ratios. Again, McCarrick found these effects in the gap region, but not at the impeller exit [21]. Here the flow is moving out of the impeller exit, in the +z and x direction, from the suction side to the pressure side of the passage. The time delay from the wave that propagates from the turbine previously mentioned (Plane 2) is also evident in the animations. The fluid flow characteristics from the suction to the pressure side of the passage showed a distinct s-curve pattern, including higher velocities on the pressure side overall. Steeper velocity gradients were observed at the bottom of the plane than at the top.

5.2.4 Plane 5: 0.8 Speed Ratio

Plane 5 was measured 1mm from the impeller exit in the gap region. The flow pattern moved in a general trend in the gap region toward the turbine (Figure 31). The average velocity of the fluid flow was 3.5m/s. The flow magnitudes increased (+z and x direction) from the suction to the pressure side. The vector angle was generally increasing (from horizontal) as the fluid flow moved across the gap region. In the middle of the plane (approximately in the center of the passage), a band of steeper velocity gradients were observed. This is due to the turbine blade-passing effects. A section of flow (purple) smaller in magnitude on the left-hand side of the plane appear to follow the band of steeper

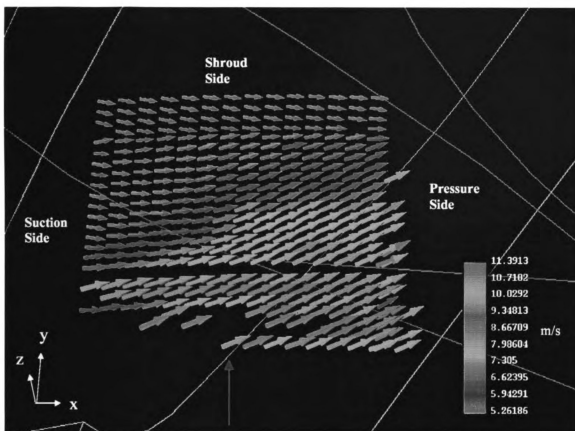
velocity gradients. There also were steeper velocity gradients observed along the bottom of the plane.

5.2.5 Plane 5: 0.4 Speed Ratio

The flow pattern moved in a general direction in the gap region toward the turbine, however this flow contained steeper velocity gradients than in the 0.8 speed ratio case (Figure 32). The average velocity of the fluid flow was 7.0m/s. As the fluid flow moved from the suction side to the pressure side (+x direction), the flow did not exhibit increasing angle with respect to the x-axis, as with the 0.8 speed ratio case. Instead, the flow moved up (+z), then down (-z) as it continued toward the pressure side. As in the 0.8 speed ratio case the middle of the plane (approximately in the center of the passage), steeper velocity gradients were observed. This also is due to the turbine blade-passing effects. In the upper left-hand corner of the plane (left of the band of blade-passing effects) vectors lower in magnitude were observed. These showed a flow that was circular in nature. There were also steeper velocity gradients observed along the lower portion of the plane.

5.2.6 Plane 5: Comparison of Both Speed Ratios

Plane 5 was measured 1mm from the impeller exit in the gap region (Figures 31 and 32). Blade-passing effects from the turbine were quite prominent. McCarrick found this condition also [21]. Although the ripple effect was present, it did not take as long for the wave to propagate back across the gap toward the impeller, as in plane 4. This would be expected since the distance to the turbine blade is less at this measured point. As with the previous cases the animation generated for this series shows these effects clearly.



Green Arrow:
Measured Perspective
White Arrow:
View Perspective

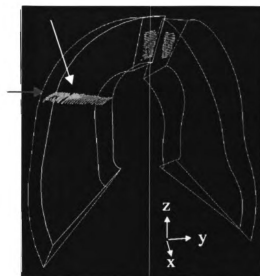
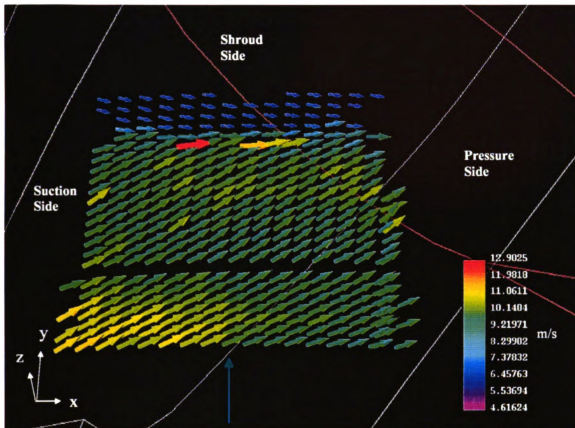


Figure 23. Plane 1 (mid-chord of impeller) at 0.8 speed ratio



Green Arrow:
Measured Perspective
White Arrow:
View Perspective

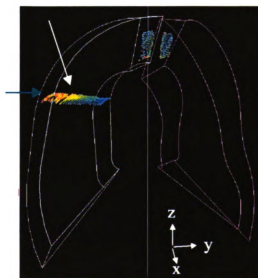
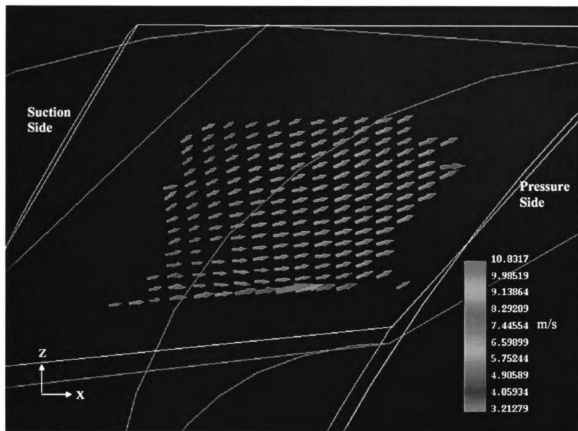


Figure 24. Plane 1 (mid-chord of impeller) at 0.4 speed ratio



Green Arrow:
Measured Perspective
White Arrow:
View Perspective

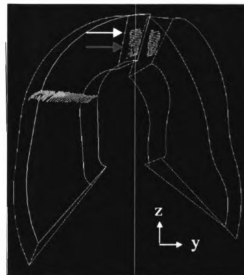
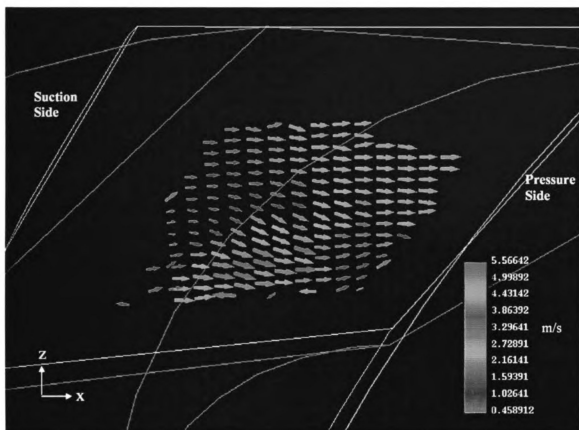


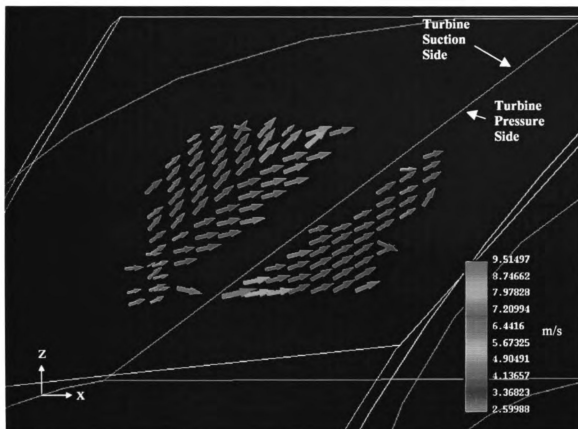
Figure 25. Plane 2 (impeller exit) at 0.8 speed ratio



Green Arrow:
Measured Perspective
White Arrow:
View Perspective



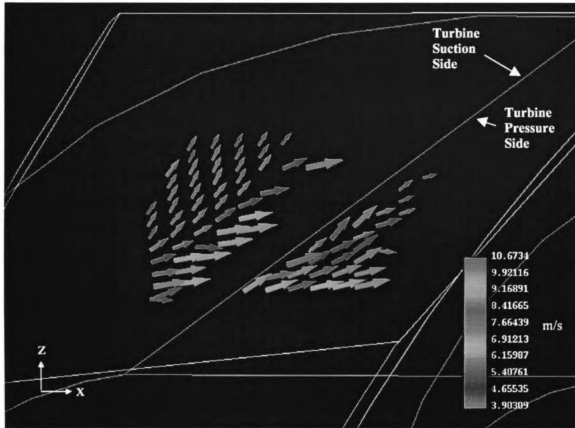
Figure 26. Plane 2 (impeller exit) at 0.4 speed ratio



Green Arrow:
Measured Perspective
White Arrow:
View Perspective



Figure 27. Plane 3 (1mm inside turbine) at 0.8 speed ratio



Green Arrow:
Measured Perspective
White Arrow:
View Perspective

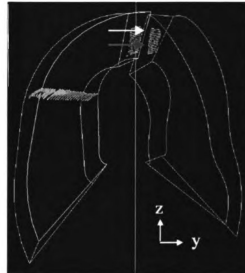
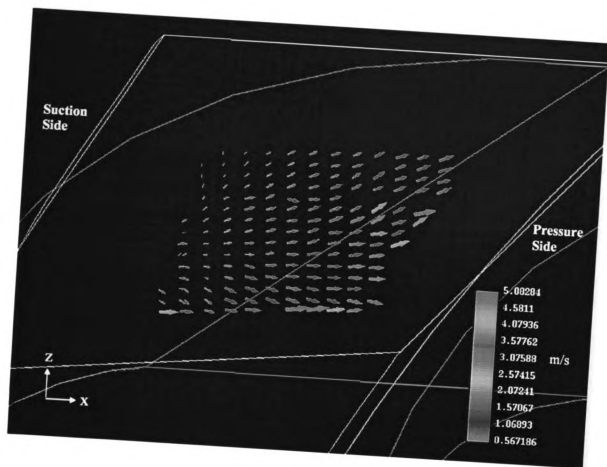


Figure 28. Plane 3 (1mm inside turbine) at 0.4 speed ratio



Green Arrow:
Measured Perspective
White Arrow:
View Perspective

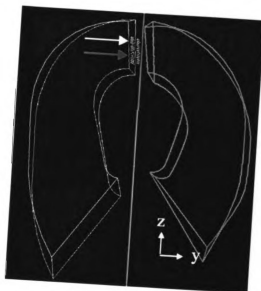
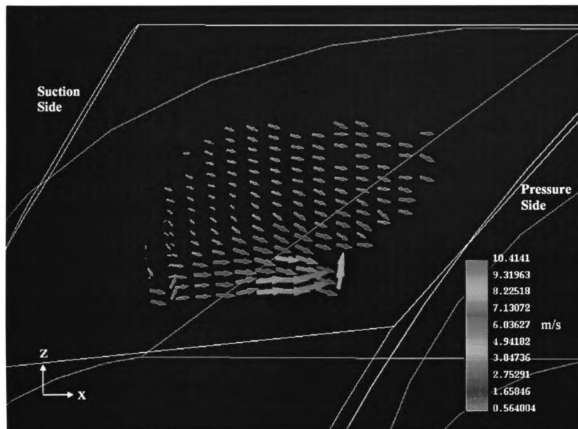


Figure 29. Plane 4 (impeller exit) at 0.8 speed ratio



Green Arrow:
Measured Perspective
White Arrow:
View Perspective

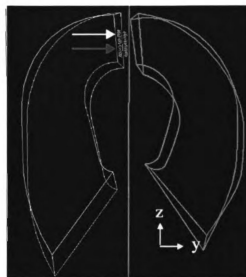
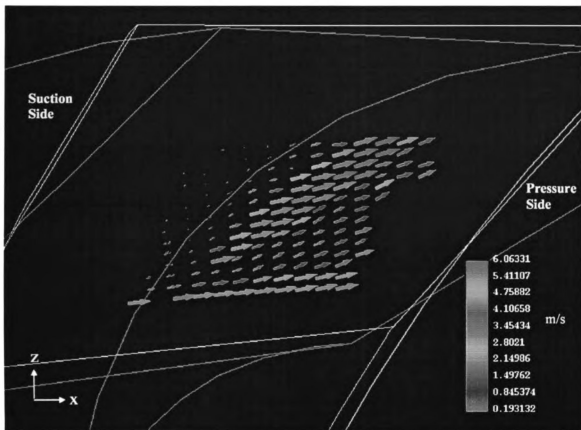


Figure 30. Plane 4 (impeller exit) at 0.4 speed ratio



Green Arrow:
Measured Perspective
White Arrow:
View Perspective

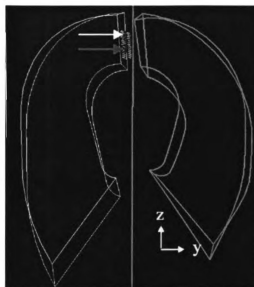
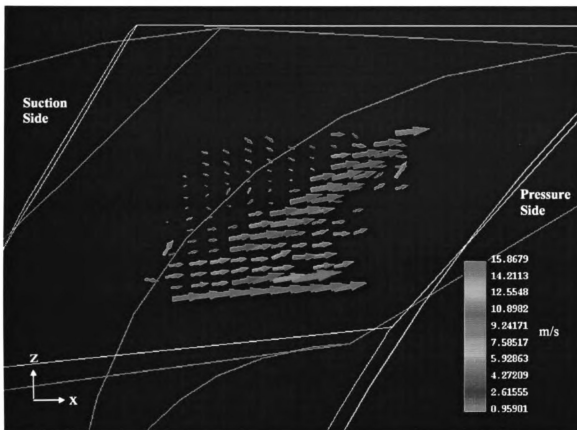


Figure 31. Plane 5 (1mm from impeller exit in gap region) at 0.8 speed ratio



Green Arrow:
Measured Perspective
White Arrow:
View Perspective

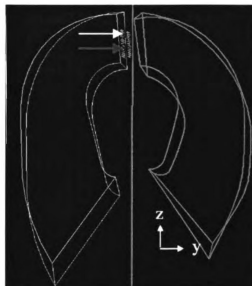


Figure 32. Plane 5 (1mm from impeller exit in gap region) at 0.4 speed ratio

5.3 Measurements with Side Window: Third Series (Planes 6-9)

5.3.1 Plane 6: 0.8 Speed Ratio

This plane was measured 2mm inside the impeller passage from the impeller exit. The average velocity of the fluid flow measured in plane 6 was 8.0m/s (Figure 33). The flow characteristics showed the main flow moving toward the exit of the impeller (+y direction), with the highest velocities occurring near the center of the passage. Velocities as low as 4.0m/s were observed in the upper left-hand corner of the plane.

5.3.2 Plane 6: 0.4 Speed Ratio

The average velocity of the fluid flow for the 0.4 speed ratio was 8.8m/s (Figure 34). The main flow also was moving toward the exit of the impeller (+y direction), with the highest velocities occurring near the center of the passage. Velocities as low as 6.3m/s were observed in the upper left-hand corner of the plane.

5.3.3 Plane 6: Comparison of Both Speed Ratios

This plane was measured 2mm inside the impeller passage from the impeller exit (Figures 33 and 34). In the impeller passage the data rate

was lower in part due to the limited optical access within the passage along with the high reflectivity from the impeller walls. A filter was incorporated in the TQANLZR code to remove the reflective data. The remaining data allowed for some flow interpretation. There was no noticeable turbine blade-passing effects found at this location. The direction of the flow measured was generally uniform for both speed ratios and followed the impeller passage (+y direction) toward the exit and turbine as expected. This toroidal flow measurement had the highest velocities occurring near the center of the impeller passage.

5.3.4 Plane 7: 0.8 Speed Ratio

Plane 7 was measured 1mm inside of the impeller passage from the exit. The average velocity of the fluid flow was 7.5m/s (Figure 35). The main flow was observed moving toward the exit of the impeller (+y direction), with the highest velocities occurring near the center of the passage. Velocities as low as 2.5m/s were observed at the top of the plane.

5.3.5 Plane 7: 0.4 Speed Ratio

The average velocity of the fluid flow for the 0.4 speed ratio was 9.0m/s (Figure 36). The main flow was observed moving toward the exit

of the impeller (+y direction), with the highest velocities occurring near the center of the passage. Velocities as low as 6.6m/s were observed along the upper left-hand corner of the plane.

5.3.6 Plane 7: Comparison of Both Speed Ratios

For plane 7, the data rate was also lower in part due to the geometry of the passage along with the high reflectivity from the impeller walls (Figures 35 and 36). As with plane 6 a filter was incorporated in the TQANLZR code to remove the reflective data. The features of the flow pattern measured were generally uniform for both speed ratios, and moved (+y direction) toward the impeller exit and the turbine as expected. The toriodal flow showed the highest velocities occurring near the center of the impeller passage with no turbine blade-passing effects at this location.

5.3.7 Plane 8: 0.8 Speed Ratio

Plane 8 was measured at the impeller exit. The average velocity for the 0.8 speed ratio case was 7.0m/s (Figure 37). A band of higher velocity vectors showing blade-passing effects can be observed diagonally along the plane. This ripple effect has a time delay that follows the turbine blade as it passes, causing the wave to propagate back across the gap region toward the impeller. A series of vectors smaller in magnitude

(3.6m/s) were observed along the top of the plane above the impeller exit. This flow is believed to be leaving the gap region, bypassing the turbine and flowing above and behind the turbine and into the lock-up clutch region. This causes a negative affect of the overall converter efficiency.

5.3.8 Plane 8: 0.4 Speed Ratio

For this plane the average velocity was 7.0m/s (Figure 38). A band of higher velocity vectors showing blade-passing effects also was observed diagonally along the plane. The ripple effect that follows the turbine blade is also evident. A series of vectors was observed along the top of the plane above the impeller exit, which were smaller in magnitude (1.1m/s) than that of the rest of the plane. This flow also is believed to be leaving the gap region and flow above and behind the turbine and into the lock-up clutch region, having a negative effect on the converter efficiency.

5.3.9 Plane 8: Comparison of Both Speed Ratios

Plane 8 was measured at the impeller exit (Figures 37 and 38). There is a generally uniform flow from the impeller exit out into the gap (+y direction). Blade-passing effects were observed for both speed ratios. The time delay (ripple effect) was also observed. The blade-passing

effects were more conspicuous in this plane than for planes 2 and 4. It may be more apparent in this case since the flow measured here is the primary flow component, whereas for planes 2 and 4 the components measured are the secondary flow. Also, for this plane the data rate was higher than that of planes 6 and 7, making the particular flow characteristics, such as blade-passing effects, more evident. This is due in part to the geometry of the impeller passage. The curvature of the passage is not as severe at the impeller exit as it is farther inside the passage, allowing for higher data rate. For the 0.4 speed ratio similar flow characteristics were observed, with the blade-passing effects a little more prominent. Also, the geometry of the converter allowed for flow to be measured above the top of the impeller passage at the exit. This can be seen in both speed ratios. The flow leaves the impeller passage and appears to flow above and behind the turbine blade into the lock-up clutch region. This flow loss will have a negative effect on the overall torque converter efficiency.

5.3.10 Plane 9: 0.8 Speed Ratio

Plane 9 was measured 1mm from the impeller exit out into the gap region. For this plane the average velocity of the vectors was 5.0m/s (Figure 39). Even with the lower data rate, a band of higher velocity flow showing blade-passing effects was observed diagonally along the plane.

The blade-passing effect appears to verify the same effect observed in the plane 5 (front window) series. A series of vectors smaller in magnitude (1.8m/s) was observed along the top of the plane above the impeller exit. This flow is believed to be leaving the gap region and flow above and behind the turbine and into the lock-up clutch region, which negatively affects overall converter efficiency.

5.3.11 Plane 9: 0.4 Speed Ratio

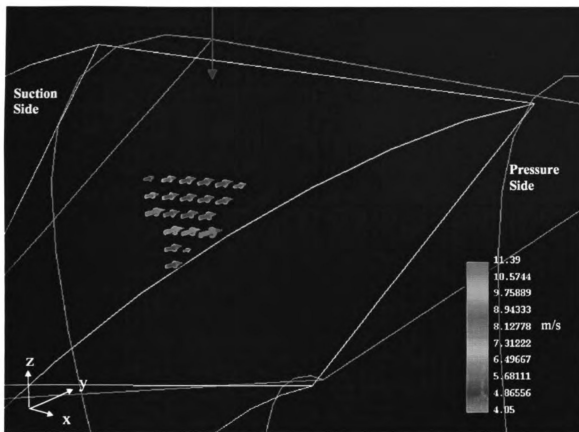
In plane 9 the average velocity was 5.4m/s (Figure 40). A band of higher velocity vectors showing blade-passing effects was observed diagonally along the plane. The ripple effect that follows the turbine blade is also evident and does not appear to be as long a time delay as with the plane 8 case. A series of vectors was observed along the top of the plane above the impeller exit, which were smaller in magnitude (1.8m/s). This flow also is believed to be leaving the gap region flowing above and behind the turbine and into the lock-up clutch region, having a negative effect on converter efficiency.

5.3.12 Plane 9: Comparison of Both Speed Ratios

Plane 9 was measured 1mm from the impeller exit out into the gap region (Figures 39 and 40). In this case the 0.8 speed ratio resulted in

low data rate. The location being 1mm out into the gap region did not create any problem with reflectivity from the impeller walls, however the problem is believed to result from the particle distribution in the fluid flow. At the 0.8 speed ratio the impeller and turbine are turning at nearly a 1:1 ratio. The fluid flow characteristics are mainly toroidal in nature at that speed ratio, therefore there would be little, if any mixing of the particles in the flow. The fluid flow does follow the passage straight out into the gap region (+y direction), as expected. The vector magnitude of the data does change in a diagonal pattern showing the blade-passing effects along the center of the passage.

In the 0.4 speed ratio case there is much more data than in the 0.8 case. This is due to the better mixing of the particles in the fluid flow. The turbine blade-passing effects are more apparent in the 0.4 case as well. The blade-passing effects are clearly evident showing the ripple effect from the turbine blade as it passes. As with the previous side window planes the flow is generally uniform across the measured area with toroidal flow (+y direction) out into the gap region.



Green Arrow:
Measured Perspective
White Arrow:
View Perspective

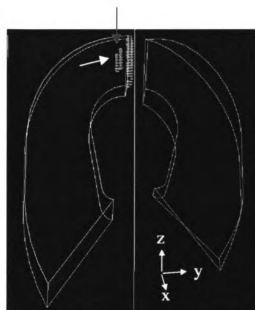
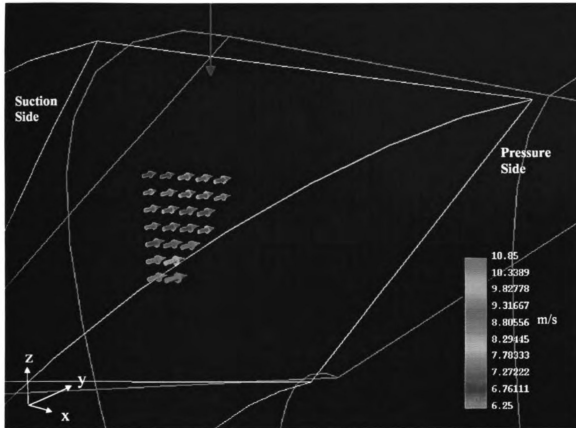


Figure 33. Plane 6 (2mm inside impeller) at 0.8 speed ratio



Green Arrow:
Measured Perspective
White Arrow:
View Perspective

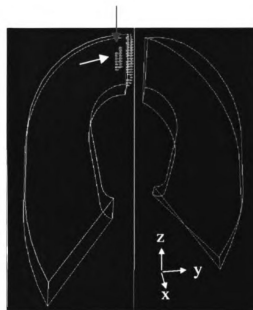
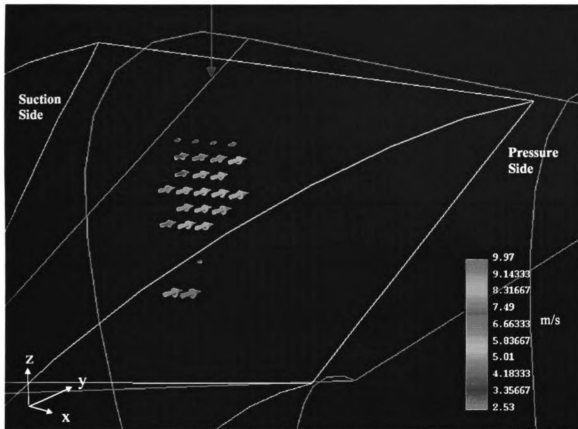


Figure 34. Plane 6 (2mm inside impeller) at 0.4 speed ratio



Green Arrow:
Measured Perspective
White Arrow:
View Perspective

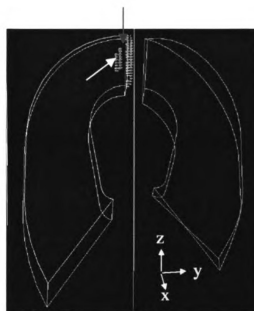
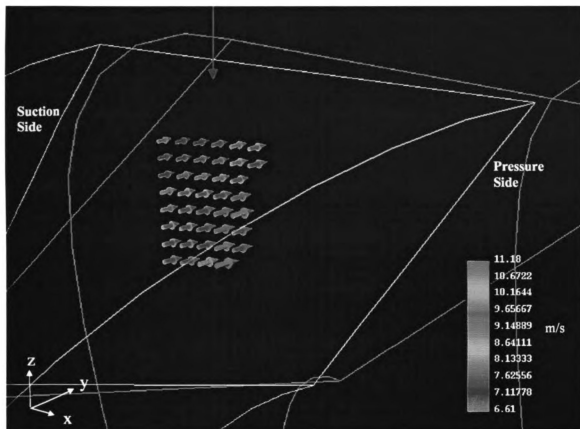


Figure 35. Plane 7 (1mm inside impeller) at 0.8 speed ratio



Green Arrow:
Measured Perspective
White Arrow:
View Perspective

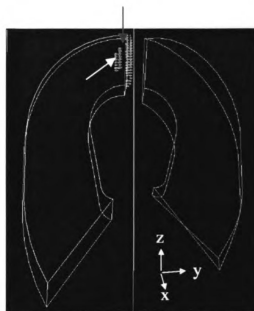
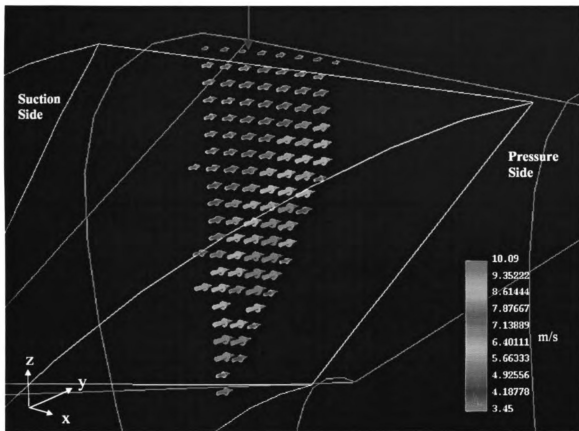


Figure 36. Plane 7 (1mm inside impeller) at 0.4 speed ratio



Green Arrow:
Measured Perspective
White Arrow:
View Perspective

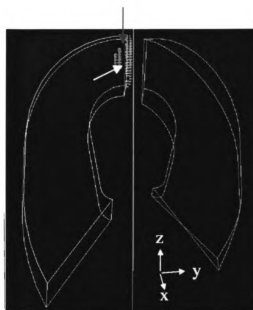
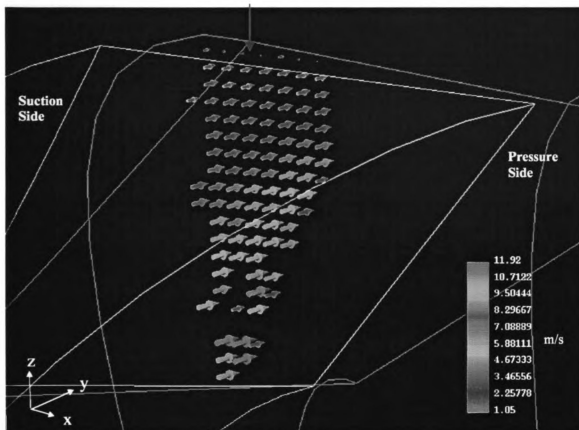


Figure 37. Plane 8 (impeller exit) at 0.8 speed ratio



Green Arrow:
Measured Perspective
White Arrow:
View Perspective

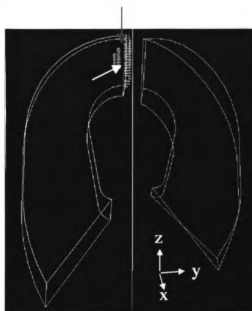
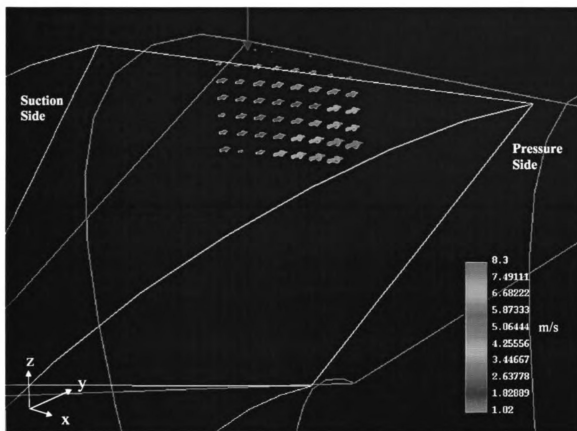


Figure 38. Plane 8 (impeller exit) at 0.4 speed ratio



Green Arrow:
Measured Perspective
White Arrow:
View Perspective

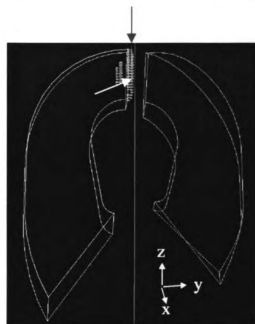
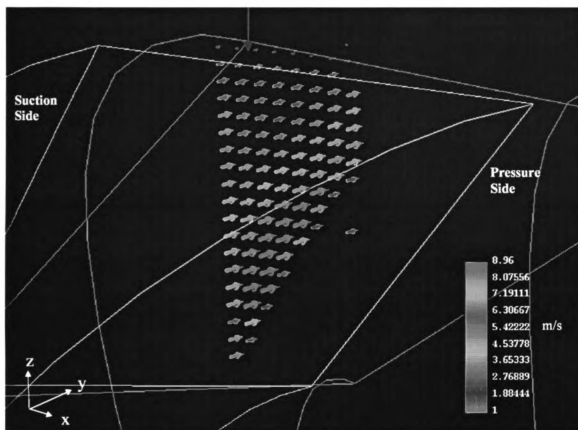


Figure 39. Plane 9 (1mm from impeller exit in gap region) at 0.8 speed ratio



Green Arrow:
Measured Perspective
White Arrow:
View Perspective

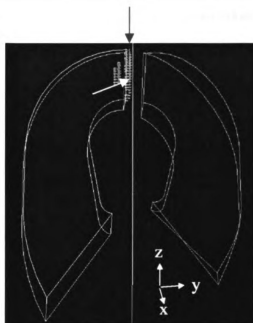


Figure 40. Plane 9 (1mm from impeller exit in gap region) at 0.4 speed ratio

5.4 Data Comparison

5.4.1 Front Window: Comparison Planes 2 and 4 at Both Speed Ratios

The front window data measured at the impeller exit, plane 2 was similar to the data measured at the same location for plane 4 (Figures 41 and 42). The animation showed blade-passing effects, which were noticeable in both series. It is noted that blade-passing effects were much more noticeable in the plane 1mm outside the impeller passage (plane 5) than in either plane 2 or 4. This would be expected with the time delay and viscous losses taken into account.

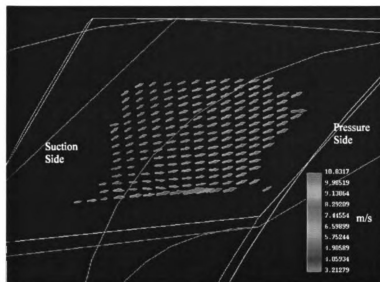
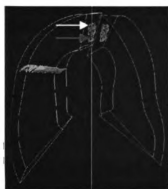
The overall flow featured shown in planes 2 and 4 were similar. More specifically, the comparisons of the results in plane 4 contained steeper velocity gradients (particularly at the bottom of the passage) than in plane 2 for both speed ratios. For the 0.4 speed ratio case, flow magnitudes were quite similar for both planes. However, for the 0.8 speed ratio case the flow magnitudes were larger in the plane 2, and were much more of a general uniform flow. This may be due, in part, to position differences between the two planes when measured.

The location of plane 2 may be slightly outside the impeller passage while plane 4 may be located slightly inside. That position difference may be large enough to show these differences in the results. The exit of the impeller passage is a very location sensitive area, in that the velocity

magnitudes change rapidly with spatial location. There are uncertainties that must be included, such as the time difference between the measured planes, which included disassembly of the converter for periodic maintenance. Also the refractive index, temperature effect, vibration, and measurement volume should be taken into account. Planes should be measured on both sides of plane 2 and 4 (inside and outside of the impeller exit) to gain further understanding on the characteristics of the fluid flow in these areas. This would provide data in a more volumetric fashion.

Another area of data to be analyzed further is planes 1 and 4, which are located mid-chord of the impeller passage and impeller exit, respectively. The flow trends found on the shroud side of planes 1 and 4 show that flow differences other than the primary flow exists in that area (Figure 43). This flow characteristic may be connected all the way through the impeller passage, possibly influenced by the reintroduction of fluid in the slots in the shroud where the tabs secure the blade. This region, as well as other regions need further investigation.

**Plane 2
1st Series**



**Plane 4
2nd Series**

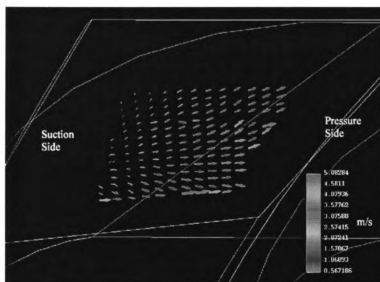
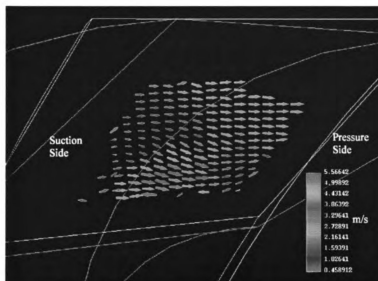


Figure 41. Comparison of planes 2 and 4 (both located at impeller exit) at 0.8 speed ratio

**Plane 2
1st Series**



**Plane 4
2nd Series**

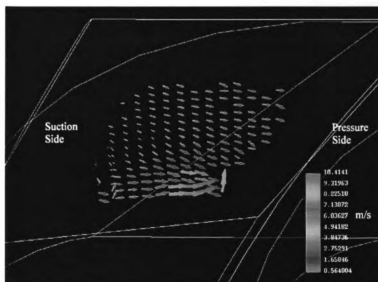
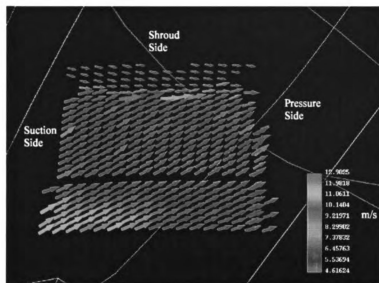
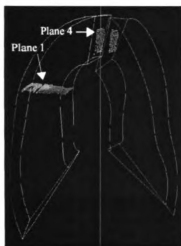


Figure 42. Comparison of planes 2 and 4 (both located at impeller exit) at 0.4 speed ratio

Plane 1
0.4



Plane 4
0.4

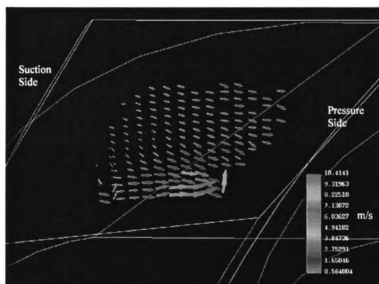


Figure 43. Comparison of planes 1 and 4 at 0.4 speed ratio

5.5 Steady State Condition Velocity Analysis

Another important task of this study was to provide useful information for CFD code development and to compare with CFD results. CFD codes have been developed to predict the internal flow characteristics in the automotive torque converter [8-12]. In general, CFD codes are calculating the flow velocities regardless of the turbine blade locations. The flow velocities from the CFD code are calculated when the impeller and turbine rotation speeds are fixed. This type of velocity profile can be defined as a steady state condition velocity analysis of the internal flow of a torque converter.

In the animated series the measured velocity clearly shows the velocity profile at any point in the converter, which varies with respect to the location of the turbine blades. The velocity has a periodic oscillation that depends on the relative locations between the impeller and turbine blades. Because of this periodic oscillation nature of the internal flow, the measured velocity cannot be compared with that of the CFD results. For this purpose the steady state condition velocities were calculated by means of averaging the measured velocities over the complete range of the turbine rotation. Therefore, the steady state condition velocities do not depend on the relative locations between the impeller and turbine blades, which is similar to velocity profiles from the CFD simulation. The advantage is the average flow rate in meters per second can be estimated

and used to gain a perspective of the overall fluid flow measured. The disadvantage is distinct flow characteristics, such as blade-passing effects at and beyond the impeller planes are not clearly discernable. The averaged steady state condition velocity profiles are shown in Figures 44-61.

5.5.1 Plane 1: Comparison of Both Speed Ratios

For plane 1, which was measured mid-chord of the impeller passage, two different flow fields were observed for both speed ratio cases (Figures 44 and 45). The primary flow in the middle of the impeller passage moves in one general direction (+z and x) from the suction to the pressure side and near the shroud show the flow direction changes to the -z direction. The magnitude of the velocity vectors was smaller in the shroud area as well, as compared to that of the rest of the plane. In the 0.8 case the average velocities were 8-10m/s for the majority of the plane, whereas the shroud side showed average velocities of 5-6m/s. For the 0.4 case the average velocities were 8-10m/s with the vertical component (+z) larger in magnitude than in the 0.8 speed ratio case. For the shroud region the average velocities were 5-6m/s.

5.5.2 Plane 2: Comparison of Both Speed Ratios

For plane 2, which was measured at the exit region of the impeller passage shows flow fields were generally uniform for both speed ratio cases (Figures 46 and 47). The general the direction of the flow magnitudes (+x direction) moved from the suction side to the pressure side of the impeller. The magnitudes of the flow were smaller on the suction side of the impeller passage than that of the pressure side for both speed ratios. For the 0.8 case there are steeper velocity gradients along the bottom of the plane (+x direction) with velocities approximately 7-8m/s. The average velocities for the rest of the plane were 4-6m/s, with the smaller velocity vector magnitudes on the suction side of the passage. For the 0.4 speed ratio as the flow moved from the suction side to the pressure side of the impeller passage (+x direction), the flow magnitudes were not at a generally increasing angle (horizontal to vertical) as with the 0.8 speed ratio case. Instead, the overall flow pattern moved up (+z direction), then down (-z direction), in a type of s-curve, as it continued toward the pressure side. Average velocities were 3-6m/s with the slowest velocities near the bottom of the plane.

5.5.3 Plane 3: Comparison of Both Speed Ratios

Plane 3 was measured 1mm into the turbine passage (Figures 48 and 49). The general the direction of the flow magnitudes moved in the +z and x direction. For the 0.8 speed ratio the flow was generally uniform with average velocities of 4-6m/s. For the 0.4 case there are steeper velocity gradients along the bottom of the plane (+x direction) with velocities approximately 7-9m/s. The average velocities for the rest of the plane were 4-6m/s, with the smaller velocity vector magnitudes on the suction side of the passage.

5.5.4 Plane 4: Comparison of Both Speed Ratios

Plane 4 was measured at the impeller exit region (Figures 50 and 51). The flow pattern showed general flow direction from the suction side of the impeller passage to the pressure side. For the 0.8 speed ratio the average velocity of the fluid flow was 2-5m/s with slower velocities (purple) on the left side of the plane of 1-2m/s. The flow magnitudes increased (+z and x direction) from the suction to the pressure side, with the exception of along the bottom of the plane where the flow moved in the +x direction. In the 0.4 speed ratio case the flow contained steeper velocity gradients. Average velocities were 3-6m/s with higher velocities (orange) of 9-10m/s. For the upper half of the plane the fluid flow moved

across the impeller passage, where the vector angle was generally decreasing (-z and x direction) as the flow continued to the pressure side. For the bottom half of the plane the steeper velocity gradients moved straight across (+x) or even downward (-z) as it approached the pressure side.

5.5.5 Plane 5: Comparison of Both Speed Ratios

Plane 5 was measured 1mm from the impeller exit in the gap region (Figures 52 and 53). Similar flow pattern, as in the impeller exit region were also observed showing the general flow direction (+z and x) from the suction side of the impeller passage to the pressure side. For the 0.8 speed ratio the average velocity of the fluid flow was 2-4m/s with slower velocities (purple) on the left side of the plane of 1-2m/s. The flow magnitudes increased (+z and x direction) from the suction to the pressure side, with the exception of along the bottom of the plane where the flow moved in the +x direction. Along the bottom of the plane there were steeper velocity gradients (green) approximately 5-6m/s. In the 0.4 speed ratio case the flow contained steeper velocity gradients in the bottom half of the plane. Average velocities were 4-6m/s with higher velocities (yellow and orange) of 7-10m/s. For the upper half of the plane the fluid flow moved across the impeller passage, where the vector angle was generally straight or slightly decreasing (-z and x direction) as the flow

continued to the pressure side. The upper left-hand side of the plane contained slower velocity gradients of approximately 1-2m/s.

5.5.6 Plane 6: Comparison of Both Speed Ratios

This plane was measured 2mm inside the impeller passage from the impeller exit (Figures 54 and 55). The direction of the flow measured was generally uniform for both speed ratios and followed the impeller passage (+y direction) toward the exit and turbine as expected. This toriodal flow measurement had the highest velocities occurring near the center of the impeller passage. There were slower than average velocities (green) of 5-6m/s at the left and right upper portions of the plane for both speed ratios. For the 0.8 speed ratio the average velocities were 7-8m/s, with some steeper velocity gradients (orange) of 9-10m/s. The 0.4 speed ratio case average velocities were 9-10m/s, with the highest velocities occurring at the center of the passage.

5.5.7 Plane 7: Comparison of Both Speed Ratios

For plane 7, the measured location was 1mm inside of the impeller passage from the exit (Figures 56 and 57). The features of the flow pattern measured were generally uniform for both speed ratios, and moved (+y direction) toward the impeller exit and the turbine as expected. The

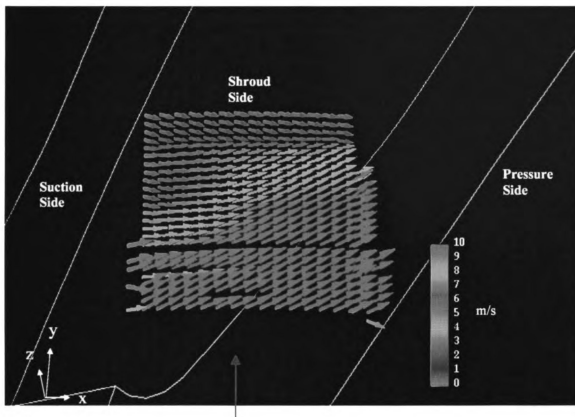
toriodal flow showed the highest velocities occurring near the center of the impeller passage. For the 0.8 speed ratio average velocities were 7-10m/s, with a line of slower velocities (green) along the top of the plane of 5-6m/s. The 0.4 speed ratio also had velocities of 7-10m/s and only a couple of slower velocities (green) occurring at the upper left-hand corner of the plane at 5-6m/s.

5.5.8 Plane 8: Comparison of Both Speed Ratios

Plane 8 was measured at the impeller exit (Figures 58 and 59). There is a general uniform flow from the impeller exit out into the gap (+y direction) for both speed ratios. The toriodal flow showed the highest velocities occurring near the center of the impeller passage. For the 0.8 speed ratio average velocities were 7-10m/s, including a line of slower velocities (green) along the top of the plane of 4-6m/s. The 0.4 speed ratio also had velocities of 7-10m/s and slower velocities (green) occurring at top of the plane at 1-3m/s. The slower velocities at the top of the plane for both speed ratios shows fluid flow leaving the impeller and continuing above the turbine, which negatively affects converter efficiency.

5.5.9 Plane 9: Comparison of Both Speed Ratios

Plane 9 was measured 1mm from the impeller exit out into the gap region (Figures 60 and 61). As with the previous side window planes the flow is generally uniform across the measured area with toroidal flow (+y direction) out into the gap region for both speed ratios. For the 0.8 speed ratio the average flow velocity was 5-6m/s. The 0.4 speed ratio has velocities of 5-6m/s, including higher velocity flow (yellow and orange) in the middle of the plane of 7-9m/s. There was a band of slower velocities along the top of the plane of 1-3m/s, for both speed ratios. This has a negative affect of overall converter efficiency.



Green Arrow:
Measured Perspective
White Arrow:
View Perspective

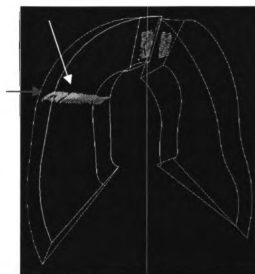
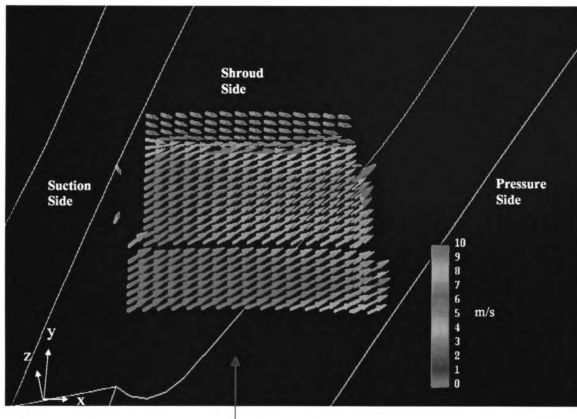


Figure 44. Steady state condition velocities plane 1 at 0.8 speed ratio



Green Arrow:
Measured Perspective
White Arrow:
View Perspective

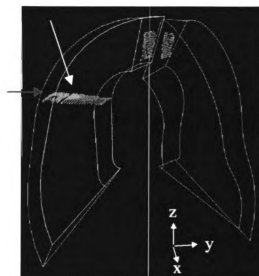
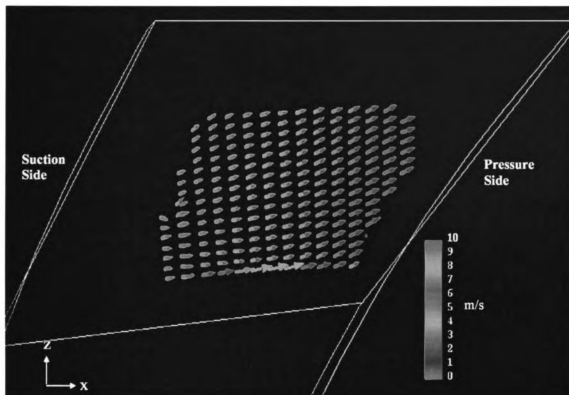


Figure 45. Steady state condition velocities plane 1 at 0.4 speed ratio



Green Arrow:
Measured Perspective
White Arrow:
View Perspective

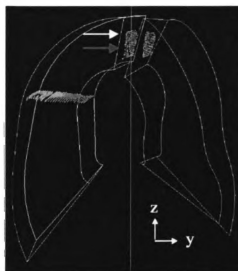
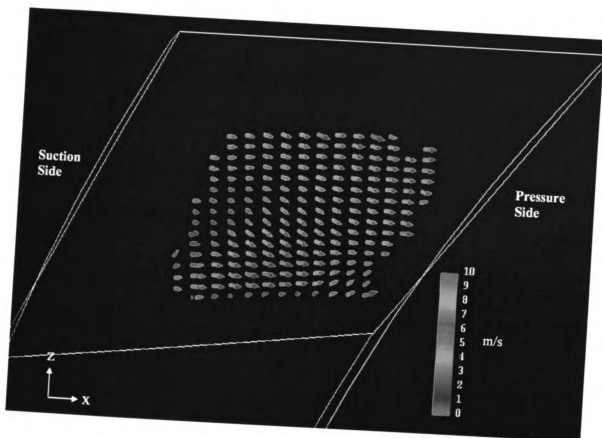


Figure 46. Steady state condition velocities plane 2 at 0.8 speed ratio



Green Arrow:
Measured Perspective
White Arrow:
View Perspective

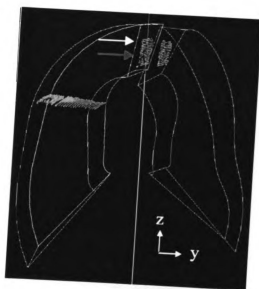
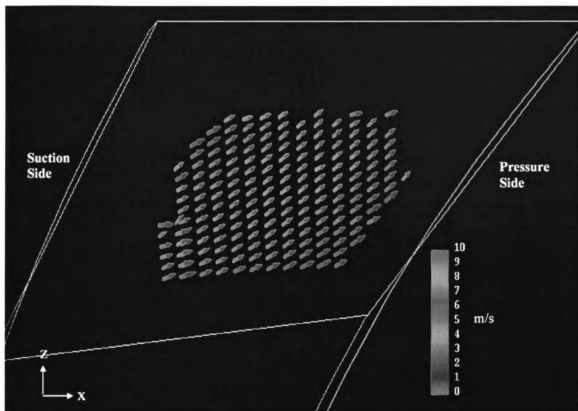


Figure 47. Steady state condition velocities plane 2 at 0.4 speed ratio



Green Arrow:
Measured Perspective
White Arrow:
View Perspective

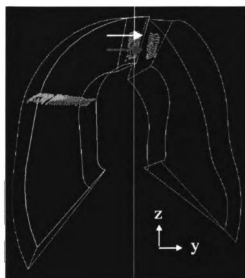
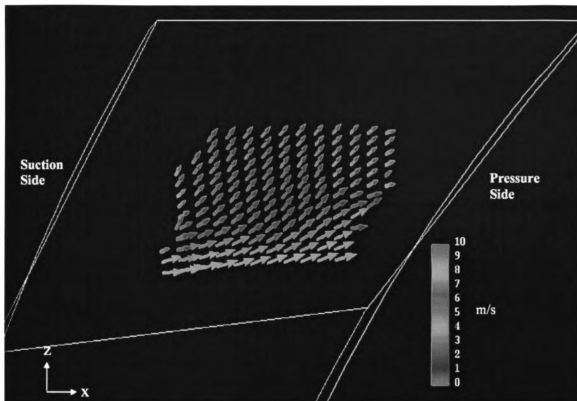


Figure 48. Steady state condition velocities plane 3 at 0.8 speed ratio



Green Arrow:
Measured Perspective
White Arrow:
View Perspective

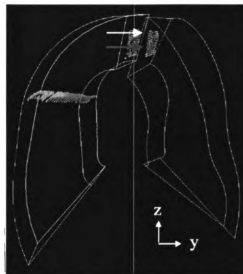
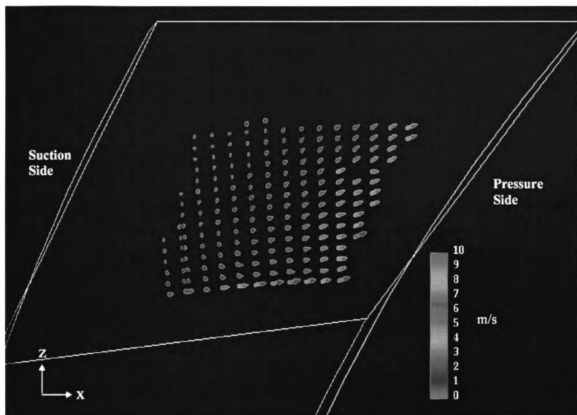


Figure 49. Steady state condition velocities plane 3 at 0.4 speed ratio



Green Arrow:
Measured Perspective
White Arrow:
View Perspective

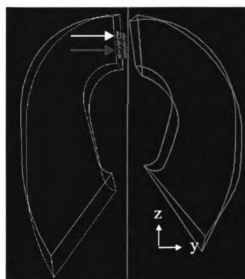
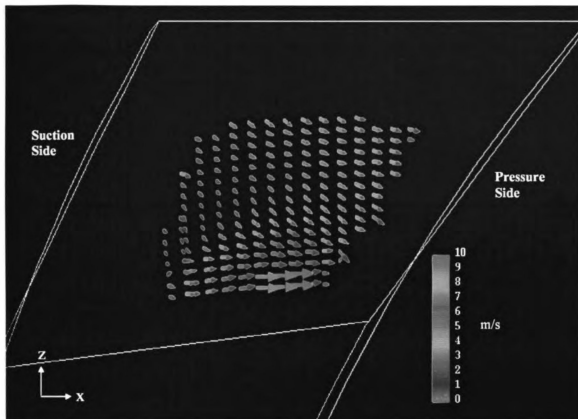


Figure 50. Steady state condition velocities plane 4 at 0.8 speed ratio



Green Arrow:
Measured Perspective
White Arrow:
View Perspective

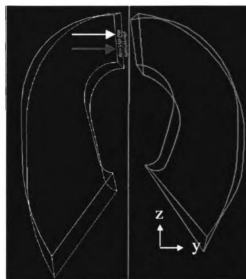
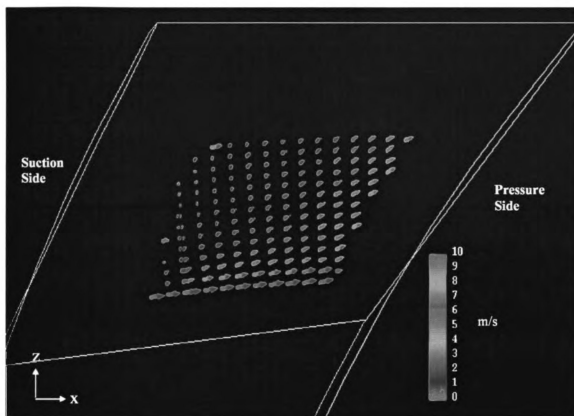


Figure 51. Steady state condition velocities plane 4 at 0.4 speed ratio



Green Arrow:
Measured Perspective
White Arrow:
View Perspective

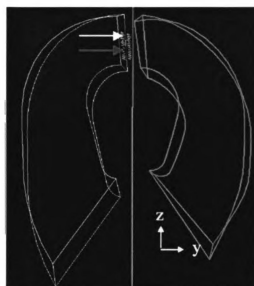
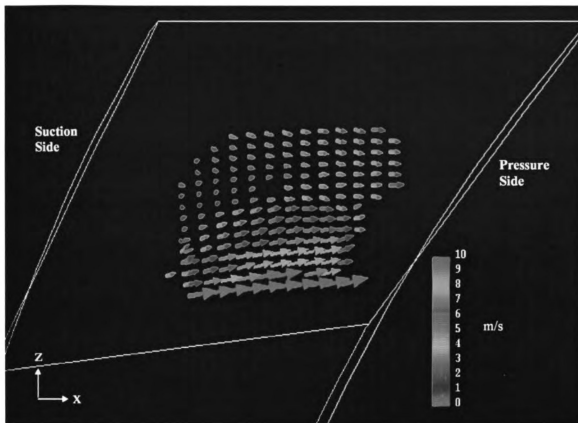


Figure 52. Steady state condition velocities plane 5 at 0.8 speed ratio



Green Arrow:
Measured Perspective
White Arrow:
View Perspective

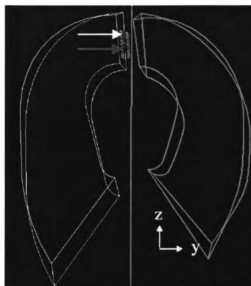
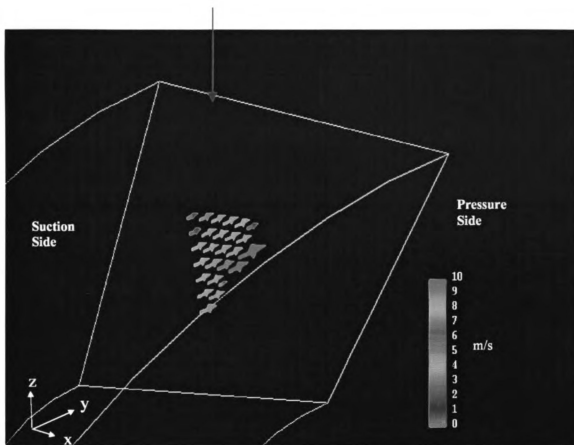


Figure 53. Steady state condition velocities plane 5 at 0.4 speed ratio



Green Arrow:
Measured Perspective
White Arrow:
View Perspective

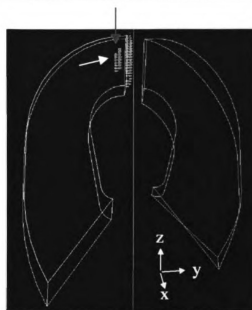
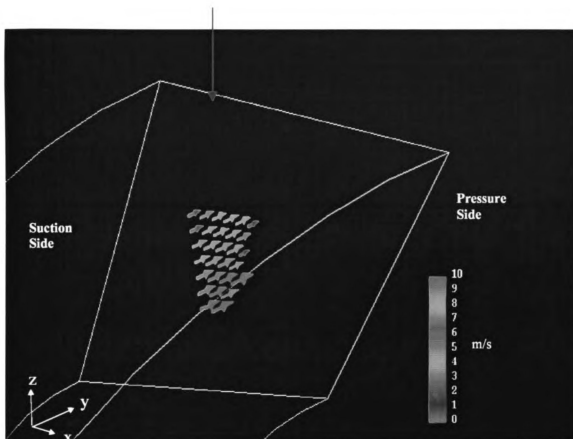


Figure 54. Steady state condition velocities plane 6 at 0.8 speed ratio



Green Arrow:
Measured Perspective
White Arrow:
View Perspective

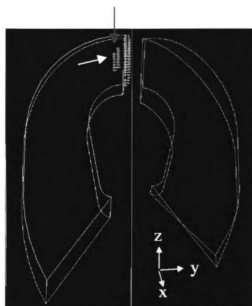
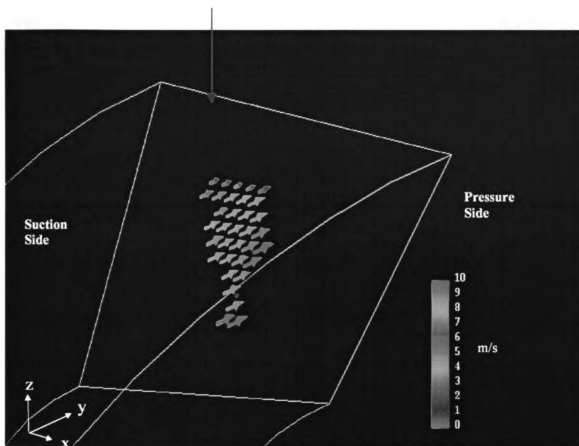


Figure 55. Steady state condition velocities plane 6 at 0.4 speed ratio



Green Arrow:
Measured Perspective
White Arrow:
View Perspective

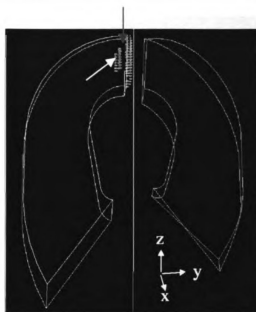
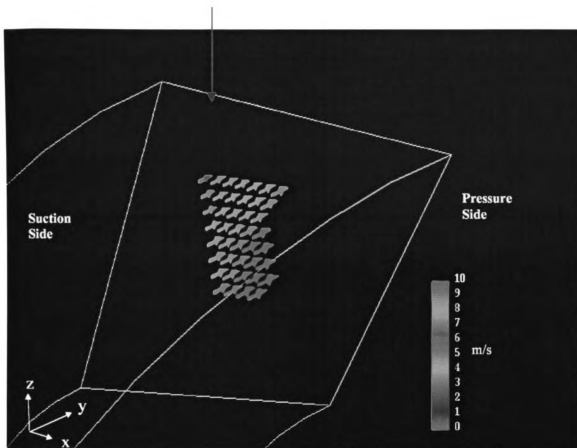


Figure 56. Steady state condition velocities plane 7 at 0.8 speed ratio



Green Arrow:
Measured Perspective
White Arrow:
View Perspective

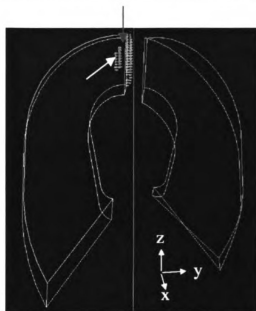
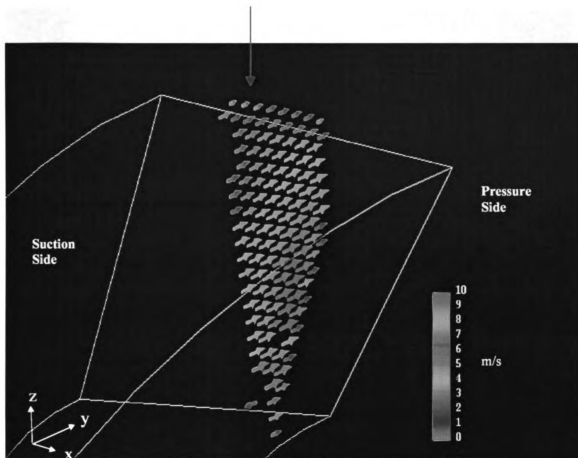


Figure 57. Steady state condition velocities plane 7 at 0.4 speed ratio



Green Arrow:
Measured Perspective
White Arrow:
View Perspective

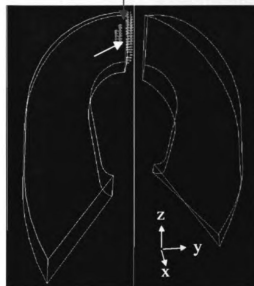
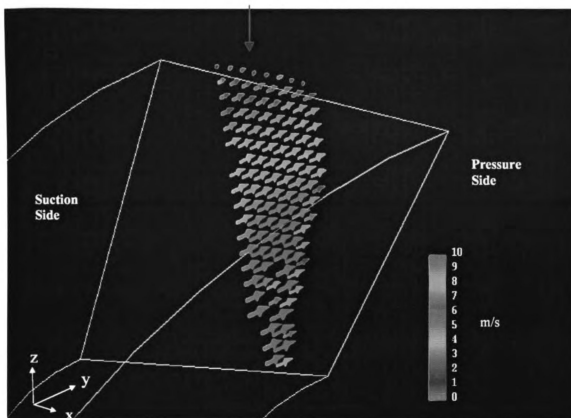


Figure 58. Steady state condition velocities plane 8 at 0.8 speed ratio



Green Arrow:
Measured Perspective
White Arrow:
View Perspective

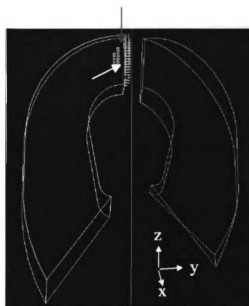
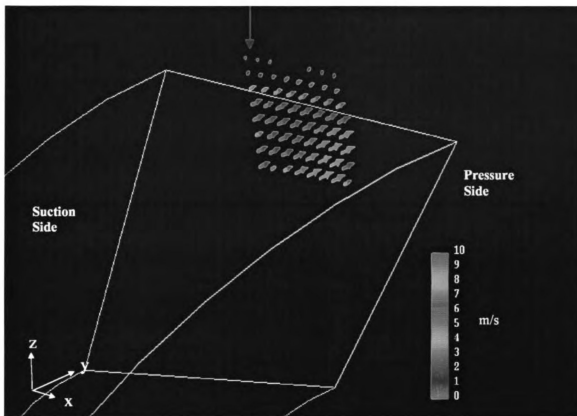


Figure 59. Steady state condition velocities plane 8 at 0.4 speed ratio



Green Arrow:
Measured Perspective
White Arrow:
View Perspective

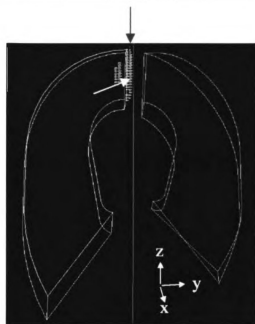
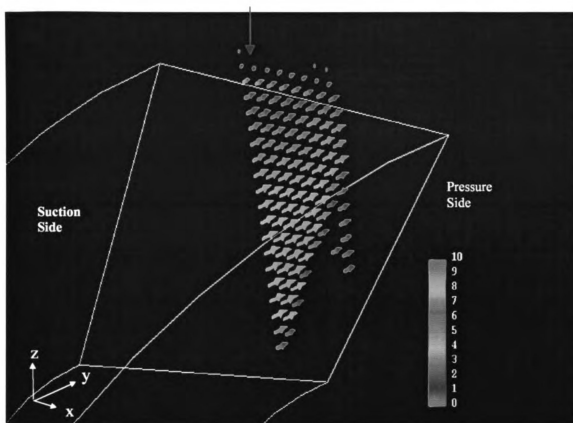


Figure 60. Steady state condition velocities plane 9 at 0.8 speed ratio



Green Arrow:
Measured Perspective
White Arrow:
View Perspective

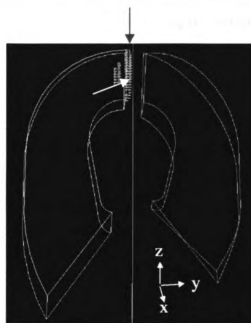


Figure 61. Steady state condition velocities plane 9 at 0.4 speed ratio

5.6 Mass Flow Rates

The mass flow rates at certain measured planes, which can also be used for CFD analysis was calculated with measured velocities. The flow through a passage of the impeller, turbine and stator was preferred to determine mass flow rates in the primary flow direction. Not all of the planes measured fit these criteria. The vertical component (+z) for plane 1 was useful for the primary flow mid-chord of the impeller passage measured in the front window. Planes 6-9 also provided primary flow characteristics measured in the side window. Planes 2-5 cannot be utilized since the components measured in these locations were not the flow direction component needed. The code Massflow was used to produce an output file, which are then plotted in turbine angle versus mass flow rate format (Figures 62-67).

The mass flow rates were used to understand the total flow variations with respect to the relative turbine locations, the fluid flow through the slots in the shroud and the region between the turbine and housing. The region in plane 9 where fluid flow loss was observed travelling out of the gap region was calculated based on the measurement velocities in plane 1 and the gap region. For the 0.8 speed ratio the flow region between the turbine and housing was estimated at 4.7%, while the 0.4 speed ratio was found to be 2.8%. Further studies need to be performed in order to understand the detailed flow characteristics in this region. Since the location of the flow was calculated 1mm outside of the

impeller exit in the gap region. Since the location of the flow was calculated 1mm outside of the impeller exit in the gap region, a plane should be measured closer to the turbine and calculations performed to see if the flow losses estimated are actually leaving the region, or reentering the turbine.

5.6.1 Mass Flow Rates: Plane 1

The mass flow rates versus turbine angle at plane 1 (measured at mid-chord of impeller passage) is shown in Figure 62. For the 0.8 speed ratio the flow ranges from 0.255-0.3kg/s. The oscillations are fairly constant per turbine angle. The 0.4 speed ratio case shows similar overall flow rate oscillations with slightly lower amplitudes of 0.475-0.523kg/s. For both speed ratio cases the flow rate increases until the turbine position is approximately 10 degrees. The flow rates are fairly uniform during the turbine positions between 10 and 18 degrees, then the flow rate decreases.

5.6.2 Mass Flow Rates: Plane 6

Plane 6 (measured 2mm inside of impeller passage from the exit) had mass flow rates of 0.255-0.3kg/s for the 0.8 speed ratio and 0.474-0.523kg/s. The oscillations of the 0.4 case showed lower

amplitudes than with the 0.8 speed ratio (Figure 63). For both speed ratio cases the flow rate increases until the turbine position is approximately 10 degrees. The flow rates are fairly uniform during the turbine positions between 12 and 20 degrees, then the flow rate decreases. For the 0.4 speed ratio the flow rate decreases between 2 and 8 degrees, then increasing, while the 0.8 speed ratio is more uniform (less sinusoidal).

5.6.3 Mass Flow Rates: Plane 7

For plane 7 (measured 1mm inside of impeller passage from the exit) the overall flow rate amplitudes were quite similar for both speed ratios (Figure 64). Flow rates were 0.12-0.158kg/s for the 0.8 speed ratio and 0.194-0.215kg/s for the 0.4 speed ratio. The flow rates decrease between 2 and 8 degrees, are fairly uniform during the turbine positions between 8 and 12 degrees, then increases to a peak between 17 and 22 degrees, then the flow rate decreases.

5.6.4 Mass Flow Rates: Plane 8

The blade-passing effects by the turbine are evident in plane 8 (measured at the impeller exit). This shows that the turbine blade-passing effects are influencing the fluid flow back through the entire gap region to the impeller exit (Figure 65). The overall flow rate amplitudes were

lower for both speed ratios as compared to Figures 63 and 64. Flow rates were 0.372-0.425kg/s for 0.8 speed ratio and 0.365-0.45kg/s for the 0.4 speed ratio. The flow rates decrease between 2 and 10 degrees, are fairly uniform during the turbine positions between 10 and 15 degrees, then increases to a peak between 17 and 22 degrees, then the flow rate decreases.

5.6.5 Mass Flow Rates: Plane 9

The blade-passing effects by the turbine are also evident in plane 9 (measured 1mm from the impeller exit into the gap region). Amplitudes were even lower here than for the other planes (Figure 66). Flow rates were 0.166-0.213kg/s for 0.8 speed ratio and 0.33-0.378kg/s for the 0.4 speed ratio. The flow rates for the 0.8 speed ratio decrease between 2 and 5 degrees, are fairly uniform during the turbine positions between 5 and 10 degrees, then increases to a peak between 20 and 25 degrees, then the flow rate decreases. For the 0.4 speed ratio the flow rate decreases between 2 and 10 degrees, then fairly uniform between 10 and 15 degrees, then increasing.

Since the area measured from plane to plane is different the mass flow rate results are particular to each plane (Figure 67). This is true even when comparing data in the same plane at both speed ratios the results are subject to different areas due to different data rates. In most

cases the planes can be compared. Plane 9 had significantly different data rates from one speed ratio to another (considerably more for the 0.4 case than the 0.8 case). Plane 1 has similar areas at both speed ratios due to close data rates and therefore can be compared to each other. Plane 8 also can be compared to both speed ratios for the same reason. Both speed ratios compared gives an indication of the different flow rates in the same plane.

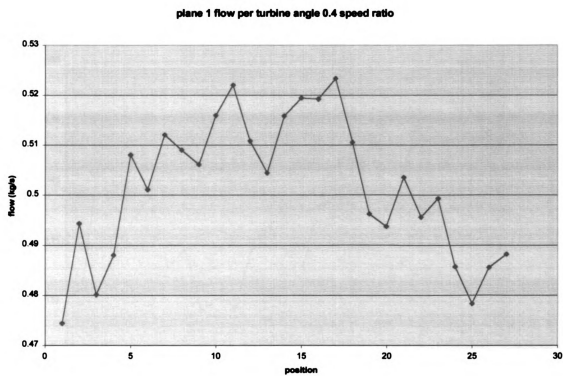
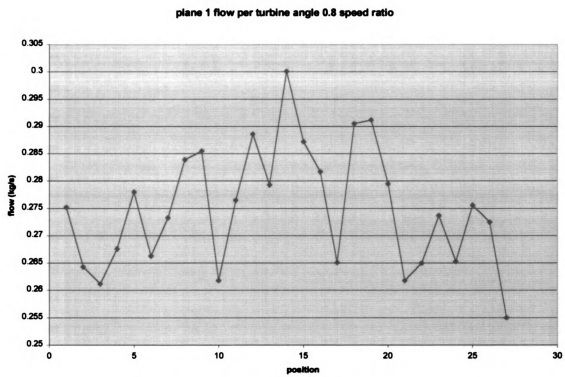


Figure 62. Mass flow rate plane 1 at both speed ratios

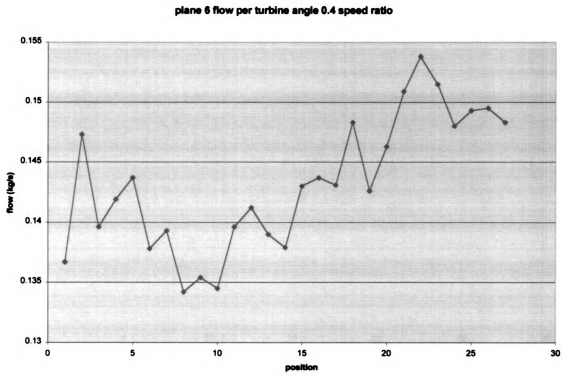
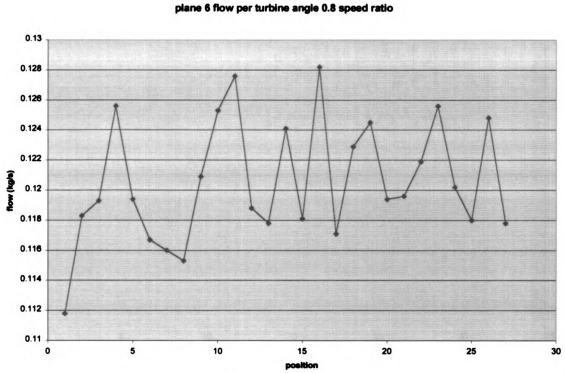


Figure 63. Mass flow rate plane 6 at both speed ratios

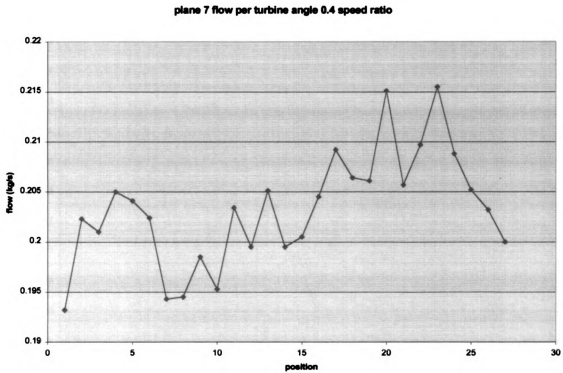
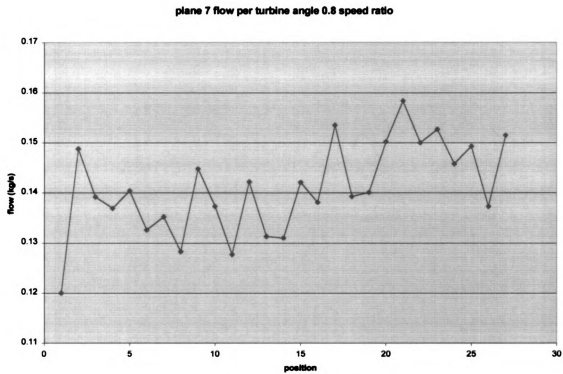


Figure 64. Mass flow rate plane 7 at both speed ratios

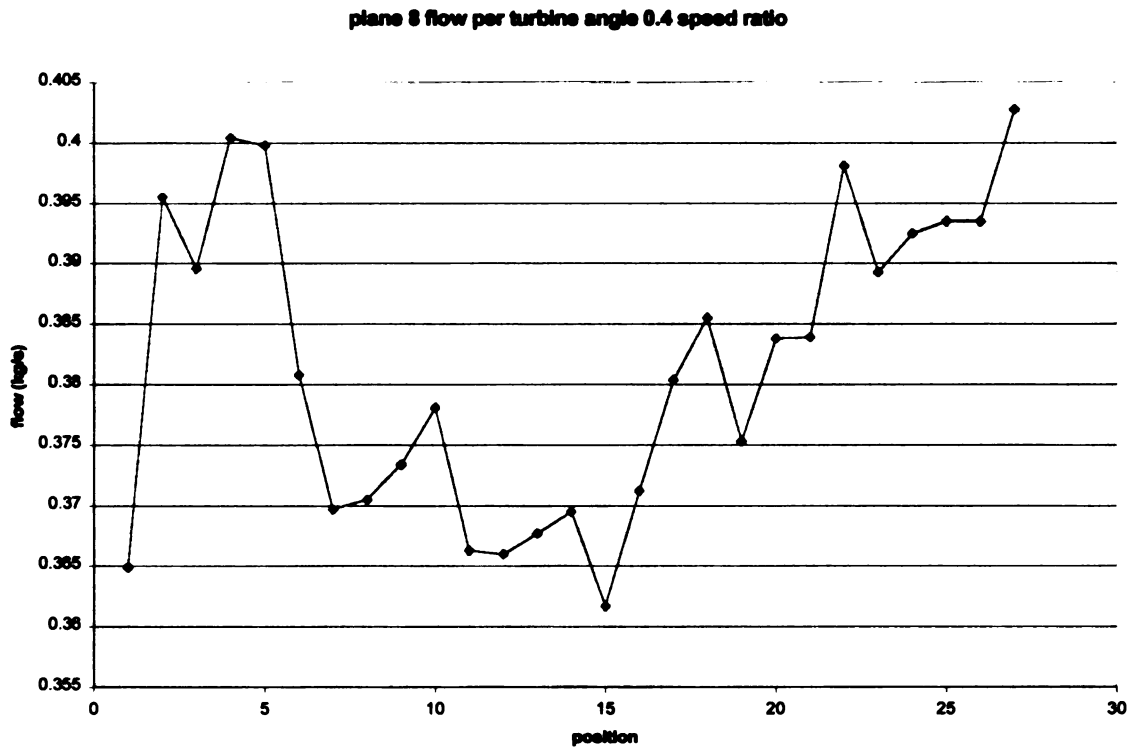
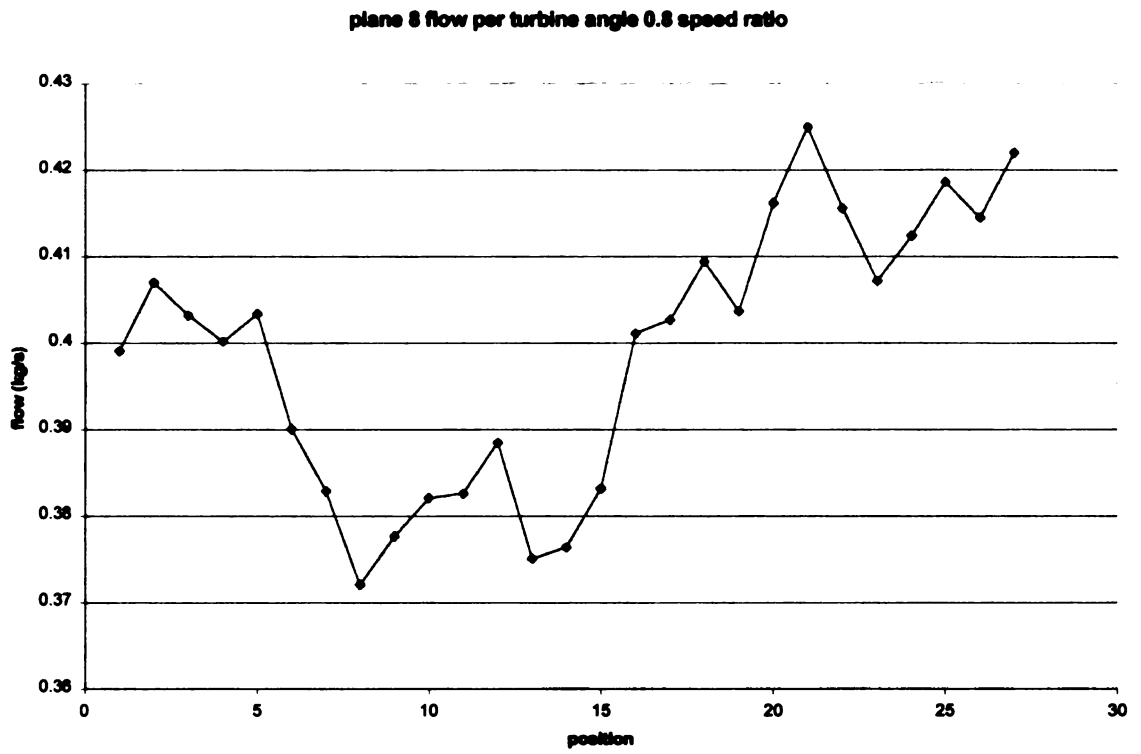


Figure 65. Mass flow rate plane 8 at both speed ratios

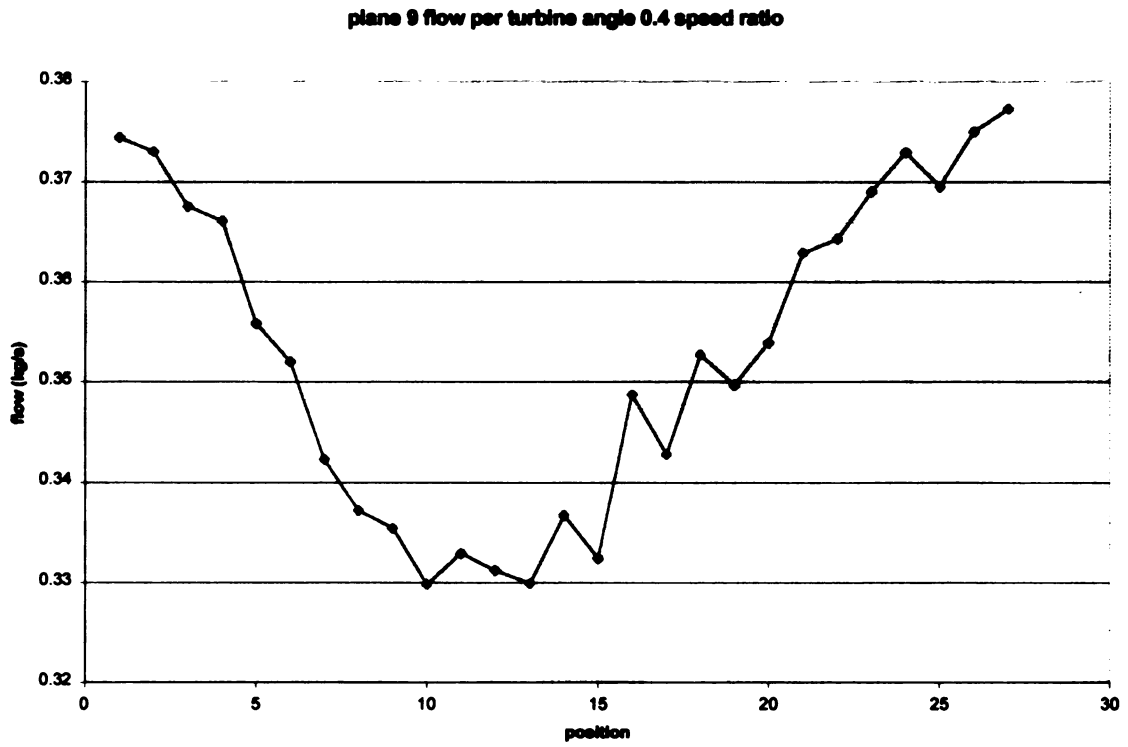


Figure 66. Mass flow rate plane 9 at both speed ratios

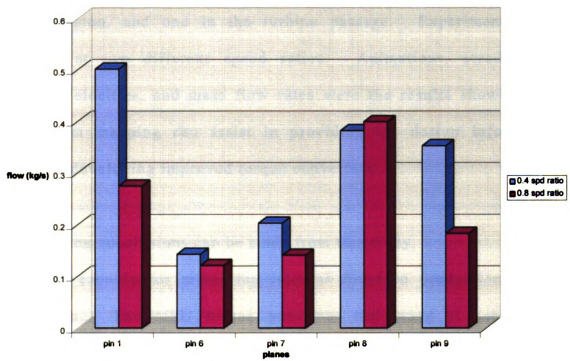


Figure 66. Mass flow rate comparison planes 1, 6-9 both speed ratios

CHAPTER 6

SUMMARY AND CONCLUSIONS

In this study the characteristics of the fluid flow were examined in an automotive torque converter. The goal was to gain an improved understanding of the complexity of the fluid flow phenomena inside a torque converter, to provide database for numerical simulation and to identify the important region locations that will benefit from additional studies. Measurements were made in a total of 9 planes. Three planes were examined in the impeller passage, three at the impeller exit, two in the gap region, and one in the turbine passage. Experiments were conducted at two different speed ratios. Animations, steady state condition velocities, and mass flow rates were the results showing that LDV system mapping can assist in providing the design information needed for developing improved torque converters.

The following conclusions can be made from this study.

- 1 LDV is capable for measuring internal flows in production torque converter. The MSU torque converter test stand is capable of providing constant temperatures, pressures, torques and flow rates needed to simulate realistic torque converter conditions.

- 2 The software animation developed by MSUERL is a powerful tool, which is used to visualize and analyze the velocity profiles. The animation results validate the post-processing algorithm (TQANLIZR) by showing that the measured velocity profile results in the correct locations without manual placement.
- 3 Turbine blade-passing effects were clearly observed in the gap region between the impeller and turbine from both the front and side window data series. This included a time delay of the turbine blade-passing effects as the wave generated during turbine blade passing propagated back toward the impeller exit.
- 4 The impeller exit area was found to exhibit high spatial and temporal velocity gradients for both speed ratios. This is evident from the data results in planes 2 and 4 that were measured at the impeller exit area.
- 5 In plane 1, at mid-chord of the impeller passage, the vertical component of flow velocities are generally uniform across the passage for the 0.4 speed ratio as compared with the 0.8 speed ratio. Also in the impeller passage, two distinct flow trends were observed, in the passage, and near the shroud, in both the 0.4 and 0.8 speed ratios.
- 6 In the turbine passage, higher velocities were observed on the pressure side then on the suction side of the turbine.
- 7 The steady state condition velocities generated showed overall flow trends of entire series in one frame.

8 Fluid flow through the gap between the turbine and converter housing was observed, which negatively affects overall converter efficiency. Flow into the region between the turbine and shell was calculated using mass flow rates to be 4.7% for the 0.8 speed ratio and 2.8% for the 0.4 speed ratio. Fluid velocity decreases as it enters the gap region from the impeller toward the turbine.

CHAPTER 7

RECOMMENDATIONS

One area that needs further fluid flow studies done is in the impeller passage along the shroud side. Flow separation here may result may result in significant loss in efficiency. There is evidence of flow patterns in the impeller passage that indicate a region of flow different than the rest of the plane measured (Planes 1 and 4). Additional planes should be measured from below plane 1 to beyond plane 4. This would provide volumetric results to help determine the full nature of these flow phenomena. Other locations such as near the shroud surface and the region around the slots that hold the blades to the shroud, need to be studied. Small perturbations of flow in these areas can result in significant turbulence generation downstream of these slots and thus, overall converter efficiency.

The following are recommendations for future studies.

- 1 Further measuring and mapping needed for additional understanding of fluid flow. An example being planes measured on both sides of impeller exit.

- 2 Include flow visualization in finding optimum locations for future LDV studies. This would help determine pertinent fluid flow locations that can be studied using LDV.**
- 3 Additional regions such as the gap region, turbine, and the region above the turbine should be investigated. Through further studies optimal distances between both the gap region (between the impeller and turbine) and the region between the turbine and shell can be determined, which can improve the overall converter efficiency.**
- 4 Windows to be fabricated and installed in the turbine blade and on the surface of the turbine side of the torque converter allowing for the study of fluid flows more in depth in that area.**

LIST OF REFERENCES

1. Lee, K., Novak, M. and Schock, H., "3-D LDV Measurement of In-Cylinder Air Flow in a 3.5L Four-Valve SI Engine," SAE Paper No. 950648, 1995.
2. Hwang, K., Lee, K., Mueller, J., Stuecken, T. and Schock, H., "Dynamic Flow Study in a Catalytic Converter Using Laser Doppler Velocimetry and High Speed Flow Visualization," SAE Paper No. 950786, 1995.
3. Hascher, H., Kasser, J., Novak, M., Lee, K. and Schock, H., "An Evaluation of Turbulent Kinetic Energy for the In-Cylinder Flow of a Four-Valve 3.5L SI Engine Using 3-D LDV Measurements," SAE Paper No. 970793, 1997.
4. Kasser, J., Hascher, H., Novak, M., Lee, K. and Schock, H., "Tumble and Swirl Quantification within a Motored Four-Valve SI Engine Cylinder Based on 3-D LDV Measurements," SAE Paper No. 970792, 1997.
5. By, R.R. and Maloney, J.E., "Technology Needs for the Automotive Torque Converter-Part1: Internal Flow, Blade Design, and performance," SAE Paper No. 880482, 1988.
6. Fister, W. and Adrian, F. W., "Experimental Researches of Flow in Hydrodynamic Torque Converters," Proceeding of the 7th Conference of Fluid Machinery in Budapest, Hungary, Vol. 1, pp. 210-224, 1983.
7. By, R.R. and Lakshminarayna, B., "Measurement and Analysis of Static Pressure Field in a Torque Converter Pump," Journal of Fluid Engineering, Vol. 117, pp. 109-115, March 1995.
8. Lakshminarayna, B. and von Backstrom, T.W., " Perspective: Fluid Dynamics and Performance of Automotive Torque Converters: An Assessment," Journal of Fluids Engineering, Vol. 118, pp. 665-676, December 1996.
9. Watanabe, H., Kurahashi, T. and Kojima, M., "Flow Visualization and Measurements of Torque Converter Stator Blades Using a Laser Sheet Lighting Method and a Laser Doppler Velocimeter," SAE Paper No. 970680, 1997.

LIST OF REFERENCES (CONT.)

10. Bahr, H.M., Flack, R.D., By, R.R., and Zhang, J.J., "Laser Velocimeter Measurements in the Stator of a Torque Converter," SAE Paper No. 901769, 1990.
11. Fax received from G.R. Becraft, Ford Motor Company Torque Converter Laboratory, Livonia, Michigan, 1992.
12. Kubo, M. and Ejiri, E., "A Loss Analysis Design Approach to Improving Torque Converter Performance," SAE Paper No. 981100, 1998.
13. Abe, K., Kondoh, T., Fukumura, K. and Kojima, M., "Three-Dimensional Simulation of the Flow in a Torque Converter," SAE Paper No. 910800, 1991.
14. Ma, W., Luo, B., and Wu, S., "The Research on Quasi-Three Dimensional Flow Design of Hydrodynamic Torque Converter Blades," SAE Paper No. 912201, 1991.
15. Ejiri, E., "A New Approach to Developing a More Efficient Torque Converter Stator," SAE Paper No. 901765, 1990.
16. Schultz, H., Greim, R. and Volgmann, W., "Calculation of Three-Dimensional Viscous Flow in Hydrodynamic Torque Converters," Transactions of the ASME, Vol. 118, pp. 578-579, July 1996.
17. Khalid, A., Legrand, J. and Robert, J.M., "Turbulent Flow Induced by an Impeller in a Closed Toroidal Loop," Journal of Fluids Engineering, Vol. 118, pp. 677-684, December 1996.
18. Gruver, J.K., Flack, R.D. and Brun, K., "Laser Velocimeter Measurements on the Pump of an Automotive Torque Converter: Part I- Average Measurements," Transactions of the ASME, Vol. 118, pp. 562-569, July 1996.
19. Gruver, J.K., Flack, R.D. and Brun, K., "Laser Velocimeter Measurements on the Pump of an Automotive Torque Converter: Part II- Unsteady Measurements," Transactions of the ASME, Vol. 118, pp. 570-577, July 1996.

LIST OF REFERENCES (CONT.)

20. Numazawa, A., Ushijima, F., Fukumura, K. and Ishihara, T., "An Experimental Analysis of Fluid Flow in a Torque Converter," SAE Paper No. 830571, 1983.
21. McCarrick, D.W., "Experimental Investigation of the Flow Field in an Automotive Torque Converter", A Thesis, Michigan State University, E. Lansing, Michigan, 1993.

MICHIGAN STATE UNIV. LIBRARIES



31293016880449